1-1-2017

Characterizing Mineral Crystallographic Preferred Orientations (cpos) Along The Eastern North American Margin In The Southern Appalachians: Implications For Middle And Lower Crustal Seismic Anisotropy

Laura Robles
Wayne State University,

CHARACTERIZING MINERAL CRYSTALLOGRAPHIC PREFERRED ORIENTATIONS (CPOS) ALONG THE EASTERN NORTH AMERICAN MARGIN IN THE SOUTHERN APPALACHIANS: IMPLICATIONS FOR MIDDLE AND LOWER CRUSTAL SEISMIC ANISOTROPY

by

LAURA ROBLES

THESIS

Submitted to the Graduate School

of Wayne State University,

Detroit, Michigan

in partial fulfillment of the requirements

for the degree of

MASTER OF SCIENCE

2017

MAJOR: GEOLOGY

Approved By:

Advisor Date

ACKNOWLEDGEMENTS

Firstly, I would like to thank my advisor Dr. Sarah Brownlee for allowing me to my research with her and for the continuous support, patience, and motivation during the time of research and writing of this thesis. Besides my advisor, I would like to thank the rest of my thesis committee: Dr. Howard, and Dr. Baskaran for their valuable comments and encouragement. My sincere thanks also goes to Matt Kohn of the Boise State University for providing the samples used in this study. Lastly but not least, I would like to thank my family and friends for supporting me throughout writing this thesis.

TABLE OF CONTENTS

LIST OF TABLES

LIST OF FIGURES

CHAPTER 1

INTRODUCTION

Seismological studies serve as a primary tool for examining the structure and mineralogy of deeper parts of the Earth (Naus-Thijssen, 2011). Seismic observations can provide valuable information regarding pressure and temperature conditions, deformation, and composition of rocks and minerals (Christensen, 1982). Most earthquake-based, or passive source, seismological studies have focused on the deep Earth, mainly the mantle. The mantle has a relatively simple composition with much less mineral diversity than the crust, and many investigations have focused on mineral structures and deformation at mantle pressure and temperature conditions. As a result, we have a better understanding of the seismic properties of the mantle than we do of the crust.

Much of our current understanding of the interior structure and composition of Earth's continental crust comes from a combination of heat flow measurements at the surface and observations of higher seismic velocities in the deep crust than in the shallow crust (Weiss et al., 1999). Based on these observations, seismologists have inferred that the lower crust is probably more mafic than the upper crust, otherwise we would expect higher heat flow at the surface, and lower seismic velocities at depth. Unfortunately, observations of seismic velocity alone are not sufficient to distinguish between many of the possible rock types and mineralogies that could exist in the lower crust. Seismic anisotropy is the directional dependence of seismic velocity, and provides the potential to differentiate between possible lower crustal rock types if the anisotropic seismic properties of those rocks are well characterized.

Seismic anisotropy has played an important role in our understanding of the structure and flow patterns in the mantle. It is broadly recognized that the largest contributor to seismic

anisotropy in the mantle is the strain-induced crystallographic preferred orientation of olivine (Long and Becker, 2010; Ward, 2010). However, in the crust, seismic anisotropy has a number of controlling factors, including the presence of aligned fractures (Naus-Thijssen, 2011), compositional layering, and the development of mineral lattice and shape preferred orientations during the progressive accumulation of strain (Okaya and Christensen, 2002; Valcke et al., 2006). Oriented cracks are not considered to be a major contributor to seismic anisotropy in the middle and lower crust because they are closed at elevated pressures. It is thus generally assumed that lower crustal anisotropy is mainly caused by mineral crystallographic preferred orientations. Understanding the causes of anisotropy in the crust is important for understanding crustal composition, structure, and formative processes (Llana-Fúnez and Brown, 2012). Inclusion of anisotropy as a variable in crustal seismic studies may help to differentiate between different rock types and fabric (Brocher and Christensen, 1990).

The seismic methods utilized to measure crustal anisotropy require an assumption of simplified elastic symmetry (Ji et al., 2015). The assumption most commonly employed is that of transverse isotropy, where there is one unique velocity axis around which all velocities are symmetric. The true elastic symmetry of most crustal rocks has not yet been characterized, and the effects of departures from transverse isotropy on seismic inversions have not been evaluated. Without a clear understanding of these factors our use of seismic observations to constrain lower crustal composition and structure is somewhat limited (Godfrey et al., 2000).

The research objective of this project is to study the factors controlling the magnitude and symmetry of seismic anisotropy in crustal rocks. We focus on two sample transects from the Blue Ridge Mountains in the southern Appalachians. Each transect contains similar amounts of two textural groups, foliated and weakly foliated rocks. We use a combination of measurements

of crystallographic preferred orientations (CPO) and mineral single crystal elastic tensors to calculate elastic tensors for our samples. The elastic tensor controls the seismic properties of materials, including seismic anisotropy and elastic symmetry, so from the calculated tensors, we can investigate the variables controlling seismic anisotropy in these rocks.

We expect deformational fabric to control the strength of the mineral CPOs and seismic anisotropy. We have three hypotheses:

1) The foliated group will have stronger mineral CPOs than the weakly foliated group. Foliated rocks have a stronger deformational fabric, thus we expect them to have stronger CPOs.
2) The northern and southern transects will have similar seismic properties. Because the two transects have similar rock types, we do not expect large variations in seismic properties related to location.
3) The foliated group will have higher seismic anisotropy than the weakly foliated group. The elastic tensor is a function of the mineral CPOs and the mineralogy of the rock. We expect the foliated group to have not only stronger CPOs, but also a higher proportion of mica minerals, which produce the highest anisotropy (Christensen, 1966).

To test these hypotheses, we will measure mineral CPOs in our foliated and weakly foliated samples from our northern and southern transects in the Blue Ridge Province of the southern Appalachians Mountains (Figure 2.1)

CHAPTER 2

GEOLOGIC BACKGROUND

For this study we used a variety of rock samples from the Blue Ridge belt in the Spruce Pine district. We chose these samples due to the fact that they are lower crustal rocks with different mineralogical composition and with fairly simple structure and geometry. We want to understand how mineral CPOs are affected by rock composition across the Blue Ridge and the implications for crustal seismic anisotropy in the southern Appalachian Mountains.

2.1 APPALACHIAN MOUNTAINS

The Appalachian Mountains include some of the most beautiful scenery in eastern North America and have a complex and distinctive tectonic history. The exposed Appalachian mountain belt ranges from Alabama to Newfoundland with buried formations that were created after the rifting of the supercontinent Rodinia (1.2 -1.0 billion years ago), and during three or more Paleozoic orogenic events: Ordovician-Silurian, Devonian Acadian and Devonian-Mississippian Neoacadian, and the Pennsylvanian-Permian Alleghenian (Hatcher, 2005). The basins deposits are characterized by sedimentary, and some volcanic rocks that were formed before the opening of the present Atlantic Ocean, and that were metamorphosed twice since the late Precambrian. The highest mountains in the entire chain with elevations exceeding 6000 ft. (Hatcher, 2005) are situated in the southern Appalachians, also known as the Blue Ridge of western North Carolina and eastern Tennessee.

2.2 BLUE RIDGE PROVINCE

The area from which our samples were collected belongs to the Blue Ridge Province in the eastern part of the ridge in North Carolina (Figure 2.1). The rocks in this area have been deformed by flexure, slip, flow folding, and thrusting. The province is divided into three major

geologic belts. The Brevard belt on the east, the Blue Ridge belt in the center, and the Unaka belt on the west. These belts are characterized by their different rock types, grade of metamorphism, and structure (Lesure, 1968).

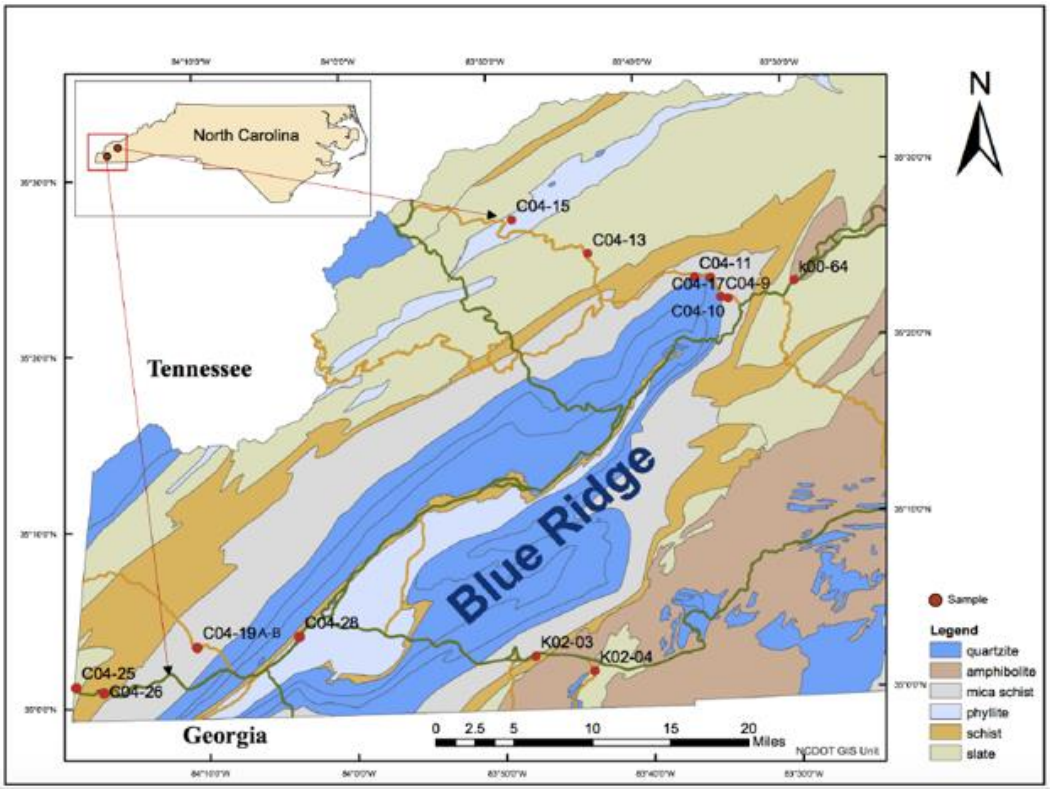

Figure 2.1. Simplified geologic map of the Blue Ridge region, including two NW-SE transects with the samples location. The blue areas are slightly different quartzites.

The Blue Ridge belt is the most extensive in the whole region and is composed of mica and hornblende rich rocks as well as younger Precambrian metasedimentary rocks. The region is usually described as a complex southwest-plunging asymmetrical synclinorium, with steeply dipping isoclinal folds on the northwest side, and gently dipping with more open folds on the southwest side (Lesure, 1968). The protoliths were probably argillaceous and quartzose sediments that have now been deformed and metamorphosed several times (Carpenter, 1970). These metamorphic events involve the formation of slip and shear cleavage as well as

retrogressive metamorphism (Hatcher, 1972). There are also lower Cambrian slates and phyllites that belong to the overlying Chilhowee Group (Hatcher, 1988).

CHAPTER 3

MATERIALS & METHODS

3.1 SAMPLES

We used a series of metamorphic rocks including schist, slate, phyllite, and metasandstone that were provided by Matt Kohn of the Boise State University Geosciences department. The samples are located within two transects across the Blue Ridge Mountains in Tennessee and North Carolina (Figure 2.1). We divided the samples into two groups based on their deformation fabric (Table 3.1), foliated and weakly foliated. The foliated group is composed of five schist samples, of which all of them except for one, K00-64, present crenulation cleavage. The weakly foliated group contains nine samples, most of which are slates and phyllites. There is one coarser-grained metasandstone as well, sample K02-03.

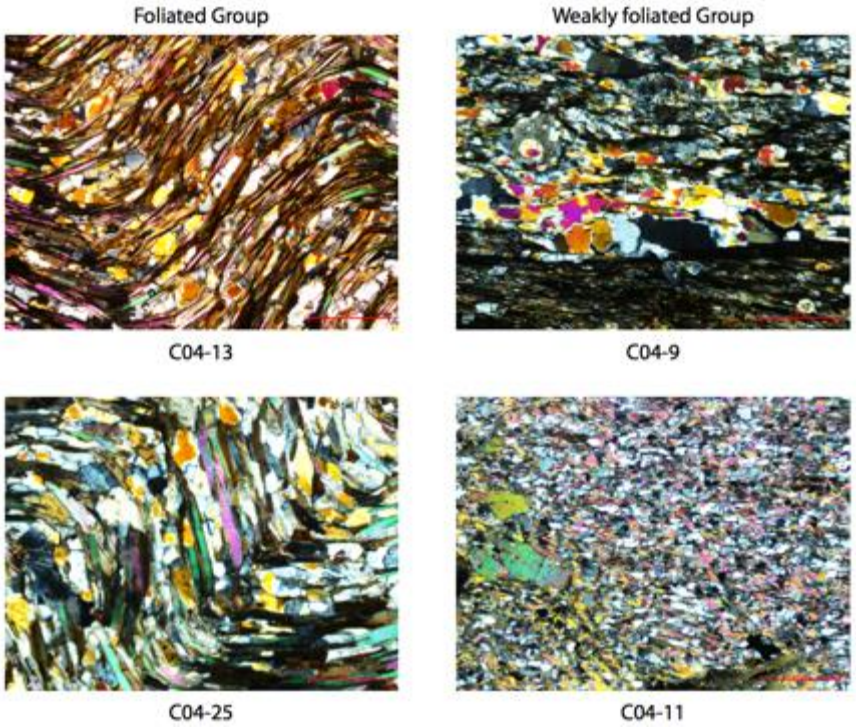

Figure 3.1. Pictures taken with a microscope camera of the foliated and weakly foliated samples. Left, schist samples with crenulation cleavage. Right, phyllites with weakly-developed foliation.

Table 3.1. Foliated and weakly foliated groups with UTM coordinates and transect division for each sample.

Sample#	Coordinates			Rock type	Transect
foliated	Zone	UTM/N	UTM/E		
K02-04	17S	250816	3878976	crenulated schist	T2
C04-26	16S	747795	3878048	crenulated schist	T2
C04-25	16S	744937	3878620	crenulated schist	T2
K00-64	17S	273690	3918810	schist	T1
C04-13	17S	252715	3922826	crenulated schist	T1
Weakly foliated					
K02-03	17S	244845	3880900	metasandstone	T2
C04-19A	16S	757361	3882886	phyllite	T2
C04-19B	16S	757361	3882886	slate	T2
C04-28	16S	767893	3884000	Phyllite	T2
C04-9	17S	266105	3917507	Phyllite	T1
C04-10	17S	265115	3919601	slate	T1
C04-11	17S	263511	3919759	Phyllite	T1
C04-15	17S	245136	3926878	Phyllite	T1
C04-17	17S	266828	3917339	slate	T1

3.2 THIN SECTION PREPARATION AND POLISHING

We prepared thin sections from each sample using standard procedures. The thin sections were oriented relative to the rock fabric such that the slide was perpendicular to the foliation and parallel to the mineral lineation when present. Crenulated samples were cut such that the thin section slide is oriented perpendicular to the foliation, and perpendicular to the crenulation lineation defined by the hinge lines of the crenulations. We used LECO silicon carbide wet or dry psa discs in the grinding process, going gradually from the highest abrasive grade #120 to the lowest #1200 until the billet was very smooth and flat. After grinding we used a combination of 10-parts Petropoxy 154 resin per 1-part curing agent to attach the billets to 46 mm x 27 mm glass slides. We used a rock saw with a horizontal blade and automatic sample holder and feeder to cut the billet from the glass at less than 1mm thickness. We again use the same progression with the grinding papers to grind the slides down to ~30 μm thick. We used a Nikon 1000 Pol

petrographic microscope to monitor thickness using quartz birefringence as an indicator during grinding. After thinning, we polished the thin sections using LECO microid diamond compound in 4 steps: 3 μm, 1 μm, ½ μm, and 1/10 μm for ~2 hours each, and with the help of a LECO automatic polisher head using 25 psi pressure. For electron backscatter diffraction (EBSD) analyses, we further polished the samples with colloidal silica for ~2 hours each. Colloidal silica polishing is unique because it provides a chemical and mechanical polish, eliminating surface and subsurface damage, which is key for obtaining EBSD patterns.

3.3 PETROGRAPHY AND POINT COUNTING

After the thin sections were made, we did a general petrographic analysis using the Nikon 1000 Pol petrographic microscope. We did routine observation in plane polarized light (PPL) and crossed polarized light (XPL) to identify minerals and specific textural characteristics, such as microstructures, and shear sense indicators, in each sample. We estimated the mineral proportions by point counting using an automated point counting stage.

3.4 ELECTRON BACKSCATTER DIFFRACTION (EBSD)

In order to understand the origin of seismic anisotropy, crystallographic preferred orientations were measured using electron backscatter diffraction (EBSD) in a scanning electron microscope (SEM). The technique uses a beam of accelerated electrons directed towards the sample surface at a low angle of 20° (Figure 3.2). These electrons enter the sample and as they exit, are diffracted by the repeating planes in the crystal structure. The diffracted electrons produce a diffraction pattern detected by a phosphor screen (Keller and Geiss, 2012). The diffraction pattern has lines called Kikuchi bands that cross at crystallographic zone axes, and are a function of the mineral phase and its crystallographic orientation in the sample. The diffraction patterns are a true projection of the geometry of the lattice planes in the crystal. The diffraction

patterns are automatically indexed using a Hough transform, which is an image processing technique that allows identification of lines and their orientations in an image. The measured patterns and detected Kikuchi bands are compared with those expected from a list of possible match units (mineral phases present in the sample). The best fit is the pattern with the lowest mean angular deviation (MAD) between the measured and predicted patterns, and this determines the most likely mineral phase and orientation of the crystal from which the measured pattern originated (Brownlee et al., 2011).

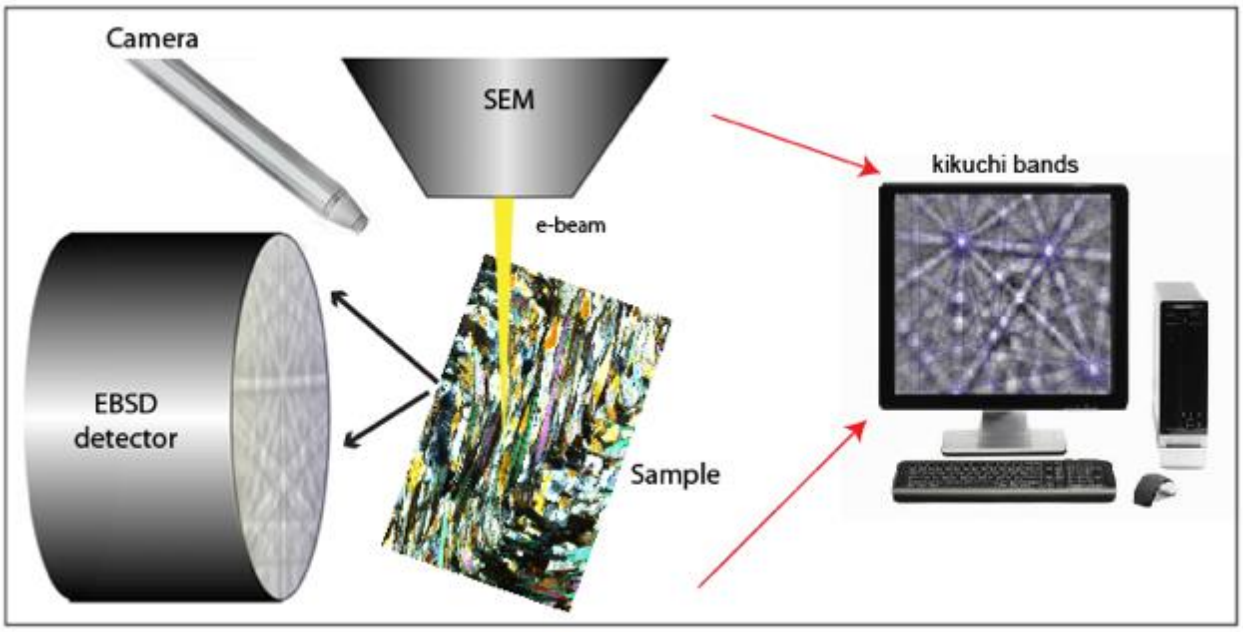

Figure 3.2. General geometric setup of EBSD. Electron beam placed on a single crystalline area of the sample surface, EBSD pattern appears on the detector and is observed by a highly sensitive camera. Data collected visualized in a computer for later processing.

Our data was collected at the University of California, Santa Barbara using a HKL Technology EBSD detector and Channel 5 software and an FEI Quanta 400f field-emission scanning electron microscope (Figure 3.3). All EBSD analyses were made conducted using the same operating conditions: accelerating voltage 20 kV, 100μm step size, spot size of 6.0. The

camera was calibrated using a silicon standard, and calibrations were refined for each sample on patterns from known quartz grains. Due to the non-conductive nature of the samples, the thin sections were coated with 4-6 nm of carbon to prevent charging in the SEM. For each sample, parameters were manually tested at the beginning of each measurement session to ensure that the diffraction patterns were correctly indexed with the corresponding minerals in each sample. Our data was collected using a mapping approach, where diffractions patterns were collected and indexed every 100 μm in a regular grid window. In general, points that are not indexed properly are found along the grain boundaries and holes where the mineral grains were ripped off during polishing. Our set of samples contained different rock types, so every sample had a unique list of minerals in the list of match units, including quartz, feldspar (plagioclase series), biotite, muscovite, chlorite, amphibole (hornblende), epidote, and garnet.

While collecting the EBSD data, we also collected energy dispersive X-ray spectrographic (EDS) data, which is used in post-processing to identify points that could have been indexed as the wrong phase. Mis-indexing occurs when the predicted diffraction pattern with the lowest MAD is not from the correct mineral. Mis-indexing is most common in geologic samples that contain a large number of phases, some of which have similar symmetries. Sample preparation can also affect EBSD indexing accuracy because the details preserved in the patterns are highly dependent on proper surface preparation. We saved EDS counts for 8 elements: Na, Mg, Al, Si, K, Ca, Ti, and Fe. The EDS counts allow us to compare the measured chemistry at each point, to the chemistry expected for the EBSD-indexed phase. We used a Matlab script that minimizes the root mean squared (RMS) difference between the measured EDS data and the chemistry of each of the possible phases in the sample to eliminate points at which the EBSD phase does not match the measured chemistry.

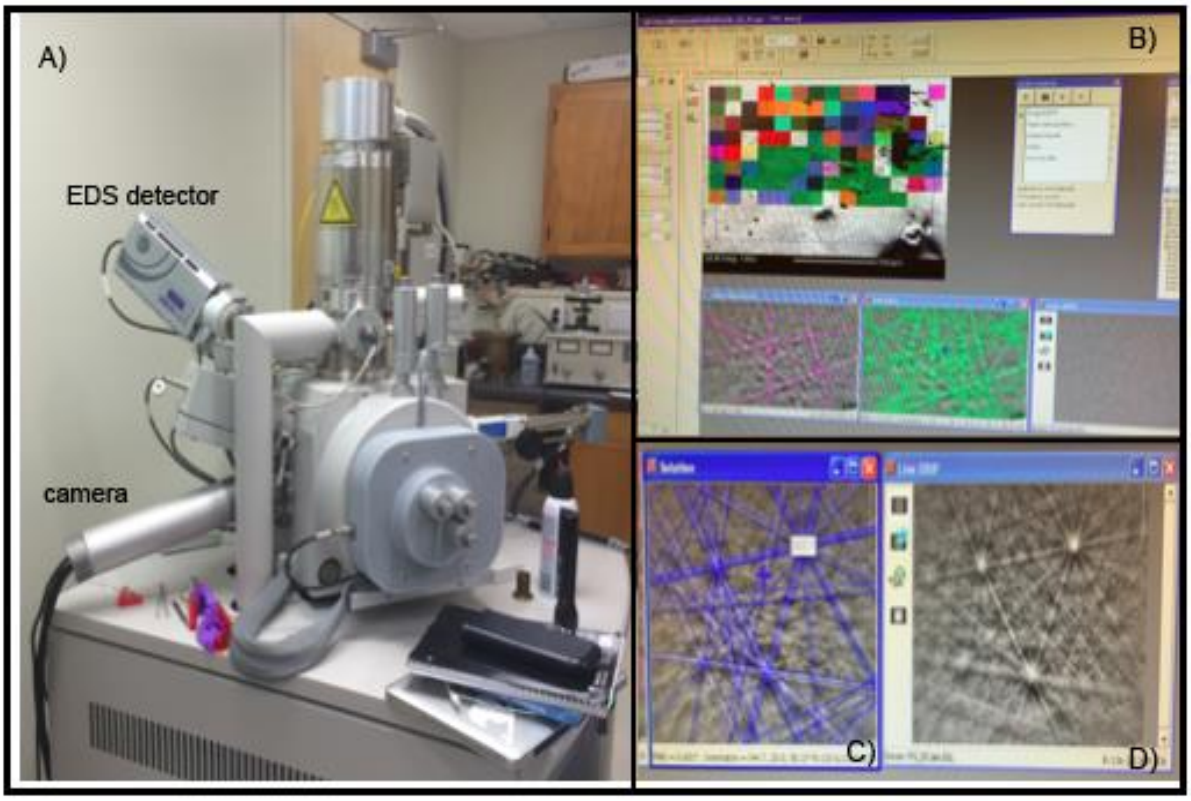

Figure 3.3. a) SEM with EBSD camera and EDS detector. B) Image of an active data collection. Each pixel color corresponds to an indexed phase and orientation. C) and D) Examples of a diffraction pattern. C) Shows the lowest MAD predicted pattern with kikuchi bands overlaid in blue.

3.5 CRYSTALLOGRAPHIC PREFERRED ORIENTATIONS

The EBSD maps give us the orientation of each crystal lattice at every point in the map. The distribution of orientations for each mineral is the crystallographic preferred orientation (CPO). We calculated an orientation distribution function (ODF) for each mineral using the MTEX Matlab toolbox (Mainprice et al., 2015). An ODF is a continuous function that fits the distribution of crystallographic orientations for each mineral. The ODF quantitatively describes the distribution of crystallographic orientations within a volume of material (Mainprice and Humbert, 1994). The texture index, or ODF-J, is a comparison between the measured orientation distribution and a uniform orientation distribution. ODF-J is a measure of the strength of the

CPO, and is highly dependent on the number of grains (N) used in the determination of the ODF. Pole figures are contoured stereonets in the samples reference frame, where areas of high density indicate that that crystallographic direction is found in that orientation more often.

3.6 ELASTIC TENSOR CALCULATION

The elastic tensors for each sample can be calculated by combining mineral single crystal elastic tensors C_{ij}, with our EBSD orientation data. Our EBSD data contains mineral phase and crystal orientation at each point in the map. We used published measurements of single crystal mineral C_{ij} and rotated them into the proper orientation at each point in the map (Brownlee et al., 2011). The rotated C_{ij} for each mineral are then averaged to produce a single mineral aggregate tensor. The single mineral aggregate tensors are then averaged with weights according to their modal proportions to calculate an aggregate C_{ij} (Mainprice, 1990). There are several possible averaging schemes, however, the most commonly used method for obtaining estimates of the effective elastic constants is the Voigt-Reuss-Hill (VRH) average (Mainprice and Humbert, 1994), which is an average of the constant strain (Voigt) and constant stress (Reuss) bounds. The end result is a volume average, which assumes that the aggregate elastic properties are a function of the elastic properties of the constituent minerals in their respective proportions. For our elastic tensor calculations, we did not include minerals with modal proportions below %5 since they have little to no effect on the final result. We also added upper and lower uncertainty bounds from Voigt and Reuss average tensors in addition to the VRH average tensor.

The elastic tensors for each sample can also be averaged together using VRH averaging to estimate regional elastic tensors, and average tensors for rock type groups. These average tensors are more likely to reflect the larger length-scales sampled by seismic wavelengths, and are calculated for comparisons with seismic observations.

3.7 SEISMIC VELOCITY AND ANISOTROPY CALCULATIONS

The calculated aggregate elastic tensors from each sample allow us to calculate the seismic properties in all possible wave propagation directions using the Christoffel equation:

$$\det\left|C_{ijkl}X_iX_J - \delta_{ik}\rho V^2\right| = 0 \qquad [1]$$

where C_{ijkl} is the elastic tensor, X_i and X_j are the direction cosines for wave propagation directions, δ_{ik} is the Kronecker delta, ρ is density, and V is seismic velocities (*Vp*, *Vs1*, or *Vs2*). *Vp* anisotropy, AVp, is the difference between the maximum and minimum *Vp* as a function of the mean *Vp*.

$$\left[(Vpmax - Vpmin)\Big/\left((Vpmax + Vpmin)/_2\right)\right] * 100 \qquad [2]$$

Vs anisotropy, AVs, is the difference between *Vs1* and *Vs2* in a particular propagation direction as a function of the mean *Vs1*. For propagation direction i, AVs is calculated as:

$$\left[(Vsli - Vs2i)\Big/\left((Vs1max + Vs1min)/_2\right)\right] * 100 \qquad [3]$$

Vs anisotropy is comparable to seismic shear wave splitting observations. *Vs1* polarization directions are the polarization directions for the fast shear wave in a particular propagation direction.

3.8 ELASTIC TENSOR SYMMETRY DECOMPOSITION

We quantified the symmetry of our elastic tensors by decomposing them into their symmetry components using the vector projection method of Browaeys and Chevrot (2004). The method involves projecting a vectorized elastic tensor on the space defined by particular symmetry components. The symmetry components are removed in order from highest to lowest-order symmetry. First the isotropic component is removed, followed sequentially by hexagonal,

tetragonal, orthorhombic, and monoclinic. After removing the monoclinic component, the remaining tensor is assigned to triclinic symmetry, which is the lowest-order possible.

CHAPTER 4:

RESULTS

Our samples were collected along two NW-SE transects within the Blue Ridge province. Within each transect we grouped the samples into two groups based on the strength of the rock fabric: foliated, and weakly foliated groups. The foliated group is composed of schist samples that present crenulation cleavage probably developed by a combination of simple shear and flattening, and includes samples K02-04, C04-26, C04-25, K00-64, and C04-13. The weakly foliated group is composed of a variety of rock types, mostly phyllites and slates that present little to any developed foliation. The weakly foliated group includes samples K02-03, C04-19A, C04-19B, C04-28, C04-09, C04-10, C04-11, C05-15, and C04-17. We grouped the samples in this way because we expect differences in seismic properties related to the strength of deformation textures. For example, we expect rocks with a well-developed foliation to have stronger crystallographic preferred orientations, and thus higher seismic anisotropy.

4.1 ROCK COMPOSITION

The modal mineral composition of each sample was determined in two ways: point counting using an automated point counting stage, and using EDS data collected during EBSD mapping. The foliated group is dominated by micas, including muscovite, biotite, and chlorite, with mica modal proportions ranging 7.9%-74%. Quartz and feldspar (plagioclase series) are the next most abundant minerals, with modal proportions ranging 10.5%-41.2%, and 12%-41.1%, respectively. The remaining 1.8%-3.7% of the rocks consists of accessory minerals including amphibole, pyroxene, garnet, and oxides (Table 4.1). All of the samples in the foliated group present crenulation cleavage, except for K00-64. The non-crenulated sample has higher proportions of quartz and feldspar than the crenulated samples.

Table 4.1. Modal mineral proportion for foliated and weakly foliated sample groups, with average and standard deviation for each mineral.

Sample#	Quartz (%)	Feldspar (%)	Biotite (%)	Chlorite (%)	Muscovite (%)	Amphibole (%)	Pyrope (%)	Epidote (%)
foliated								
K02-04(crenulated)	41.2	13.6	3.8		34.8	3.6	2.9	
C04-26(crenulated)	10.5	2.1	9.6		74.0	0	3.7	
C04-25(crenulated)	25.7	41.1	24.7		7.9	0	0.6	
K00-64	25.6	35.4	22.9		13.4	0.9	1.8	
C04-13(crenulated)	34.5	12.0	14.3		36.5	2.7	0	
average	27.5	20.8	15.1		33.3	1.4	2.2	
± s.d.	10.3	16.6	8.8		26.0	1.6	1.3	
weakly foliated								
K02-03	50.2	41.7	6.2	0	0.1	0		2
C04-19A	64.9	5.3	14.3	5.4	10.9	0		0
C04-19B	78.1	5.5	0	0	0	1.1		15
C04-28	36.2	49.6	0	14.1	0.1	0		0
C04-9A	59.4	31.7	1.1	0.5	7.4	0		0
C04-10	66.4	23.1	5.6	0	1.1	3.8		0
C04-11	39.6	23.0	0	0	37.5	0		0
C04-15	63.0	32.5	2.8	0	1.6	0		0
C04-17	64.9	8.4	10.4	5.4	10.9	0		0
average	58.1	24.5	4.5	3.2	7.7	0.7		2.1
± s.d.	13.6	15.9	5	5	12.1	1.4		5.3

The weakly foliated group is dominated by quartz and feldspar, with modal proportions ranging 36.2%-78.1%, and 5.3%-49.6%, respectively. The weakly foliated group contains much less mica than the foliated group, ranging from 6.2-37.5%. Accessory phases, including amphibole and epidote make up the remaining 3.7-15% (Table 4.1). Given the variety of rock types in this group there is not a clear modal compositional variation among these samples. In general the strength of the visible petrofabric is related to the amount of mica in the samples: the foliated group contains an average of 24.2% ± 20.7 mica, whereas the weakly foliated group contains 5.2% ± 8.1 mica on average (standard deviations were calculated from Table 4.1).

4.2 MINERAL CPOS

4.2.1 CPO strength

We used Mtex to calculate the texture index parameter of the orientation distribution function (ODF-J) as a measure of CPO strength for every mineral in each sample. The dominant minerals that will contribute to anisotropy in these rocks are quartz, feldspar (plagioclase), mica (biotite, muscovite, chlorite), amphibole (hornblende), and to a lesser extent, epidote. Garnet is present in many of the foliated samples, but garnet has cubic symmetry, and thus does not contribute to anisotropy. The remaining minerals are not abundant enough to determine CPO.

4.2.2 Quartz

Quartz has the weakest CPO in both the foliated and weakly foliated groups. The quartz CPO varies within the foliated group with average ODF-J values of 2.4 ± 0.4 (Table 4.2). Some samples display simple shear oriented roughly perpendicular to the crenulation-lineation due to the asymmetric nature of the crenulation, with a maximum concentration of [0001] located at the center of the pole figure (e.g. sample K02-04 Figure 4.1). This CPO is consistent with prism-<a> slip, which aligns the c-axes perpendicular to the shear direction within the shear plane. We also have samples where the c-axes are oriented perpendicular to the foliation, and slightly tilted, or asymmetric relative to the foliation (e.g. samples C04-25 and C04-26, Figure 4.1). This CPO is consistent with basal-<a> slip, which aligns the c-axis perpendicular to the foliation (Ji et al., 2015).

The quartz CPOs in the weakly foliated group are more consistent among the samples. CPO strength is similar for the weakly foliated group as it was for the foliated group, with average ODF-J values of 2.3 ± 0.6 (Table 4.2). The majority of the weakly foliated samples have

c-axes oriented between perpendicular to the foliation and parallel to the crenulation-lineation, which is consistent with a combination of basal-a slip and prism-a slip (Figure 4.1).

4.2.3 Feldspar (plagioclase)

Feldspar CPOs are less clear, or organized, than quartz CPOs, which makes them less straightforward to interpret in terms of crystallographic slip systems. The CPO strength is technically higher than quartz on average, with average ODF-J values of 3.3 ± 1.7 for the foliated group and 3.2 ± 1.6 for the weakly foliated group (Table 4.2). Both foliated and weakly foliated groups tend to have maxima of the (001) poles roughly perpendicular to the foliation (Figure 4.2), which would be consistent with deformation by dislocation glide on the (001) plane, which has been documented previously in feldspar (Prior and Wheeler, 1999). But the feldspar CPOs are complex, and probably indicate deformation by multiple mechanisms, and on multiple slip systems.

Table 4.2. ODF-J values for each mineral in each sample. Samples with low N count have artificially high ODF-J values, samples with N < 100 are shaded gray, and are not included in average calculations. Errors on averages are ± 1 standard deviation.

Sample#	Quartz		Feldspar		Biotite		Hornblende		Muscovite		Pyrope	
Foliated	N	ODF-J	N	ODF-J	N	ODF-J	N	ODF-J	N	ODF-J	N	ODF-J
K02-04	4834	2.7	1296	3.1	33	31.8	23	46.7	2325	5.7	42	56
C04-26	3834	2.2	657	5.5	1847	8.9			23138	2.9	20	16
C04-25	4904	2.3	5583	1.5	2190	7.8			1026	5.5	42	3.3
K00-64	3118	2.9	2550	4.5	876	10.4	10	100	1049	7.6	16	40.7
C04-13	9350	2.1	2741	1.9	1151	7.9	33	32.2	7096	4.2		
average		2.4		3.3		8.8				5.2		
± s.d.		0.4		1.7		1.2				1.8		
Weakly foliated	Quartz		Feldspar		Biotite		Epidote		Muscovite		Chlorite	
	N	ODF-J	N	ODF-J	N	ODF-j	N	ODF-J	N	ODF-J	N	ODF-J
K02-03	8831	3.1	5008	1.9	631	16.9	336	5.47	4	248.9		
C04-19B	11528	1.8	650	4.3			2693	1.9				
C04-28	11831	2.3	15288	1.3					38	27.4	6098	12.0
C04-9A	10535	2.7	3570	1.8	11	93.3			81	14.0	3	331.9
C04-10	8779	3.1	493	5.5	24	45					7	142.4
C04-11	4703	1.3	693	4.8					1545	6.1		
C04-15	5721	2.2	2515	2.5	54	22.6			115	12.5		
C04-17	11902	2.2	921	3.4	361	12.6			422	5.7	365	8.9
average		2.3		3.2		14.7		3.7		8.1		10.4
± s.d.		0.6		1.6		3.0		2.5		3.8		2.2
Weakly foliated Hornblende	C04-19B		N	123	ODF-J 20.2							
	C04-10		N	29	ODF-J 38.1							

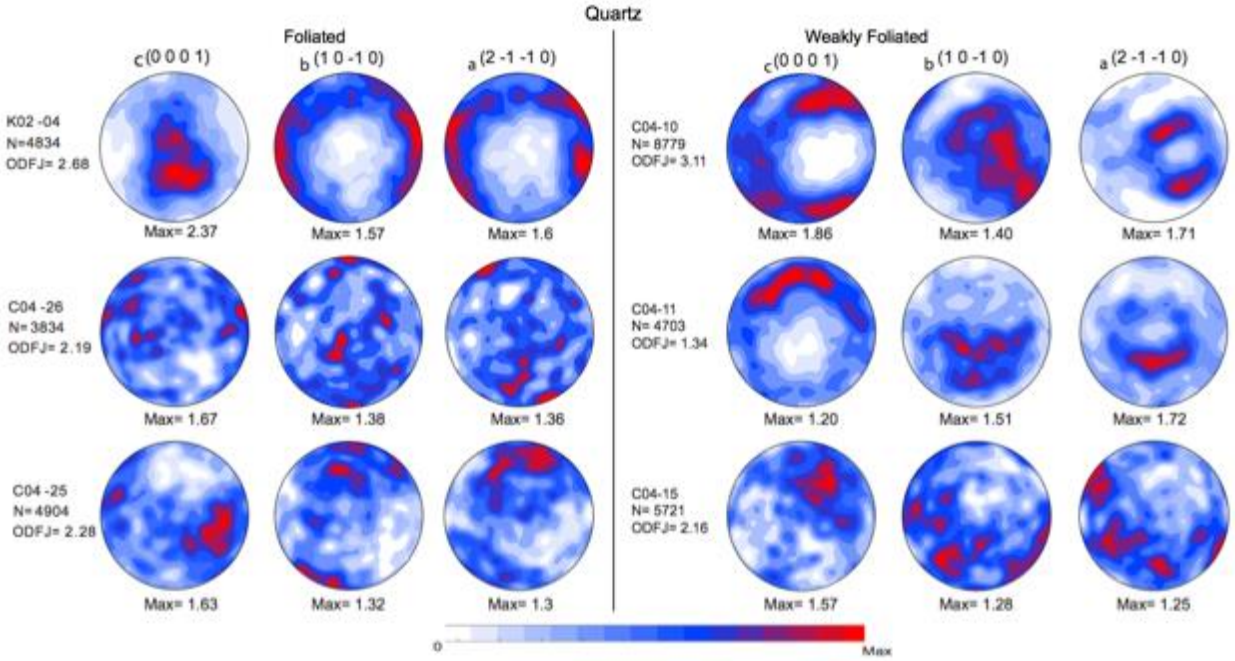

Figure 4.1. Pole figures of quartz. Left, foliated group. Right, weakly foliated group.

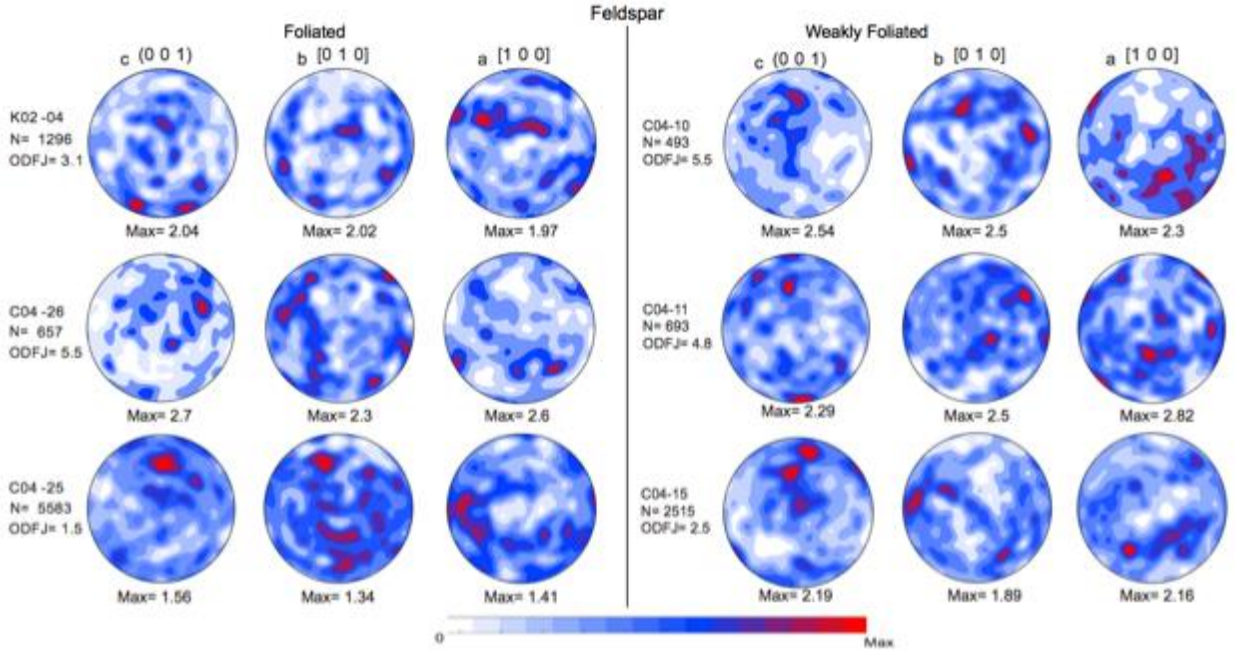

Figure 4.2. Pole figures of feldspar. Left, foliated group. Right, weakly foliated group.

4.2.4 Micas (biotite, muscovite, chlorite)

Mica CPOs are the strongest of all the minerals with average ODF-J ranging 5.2-14.7 (Table 4.2). All three micas have similar CPOs in both groups, with a (001) point maxima perpendicular to the foliation, and girdle distributions of [100] and [010] within the foliation. Many of the samples have maxima of [010] within the girdle distribution parallel to the crenulation lineation. This CPO is not unusual for micas that typically slip in any direction within the basal plane of the mineral on the (001) [hk0] slip system (Figure 4.3).

The muscovite CPOs reflect the crenulation in the foliated samples, displaying bimodal distributions of (001) poles, with the stronger maxima perpendicular to the overall foliation (Figure 4.3). Muscovite also displays a cross girdle of [010] and [100] directions in the crenulated samples (Sample C04-13, Figure 4.3). Samples that don't have bimodal (001) distributions or [010] cross-girdles, display spreading of the (001) maxima, and spreading of the girdle distributions of [010] and [100] (Sample C04-25).

The biotite in the weakly foliated group has the strongest CPOs on average, and displays distinct maxima of (001) poles perpendicular to the foliation. There is a maximum of [010] directions roughly parallel to the lineation, suggesting slip on (001) [010] (Figure 4.3) (Erdman et al., 2013).

4.2.5 Amphibole (hornblende)

Most of the samples in the foliated group do not have enough hornblende points to give accurate CPOs as we can see in Figure 4.4. However, one weakly foliated sample has a clear hornblende CPO with only 123 separate grains indexed. This CPO is relatively straightforward to interpret with (100) poles perpendicular to the foliation, and [001] directions parallel to the lineation. This CPO is consistent with the most common slip system in hornblende, (100)[001]

(Figure 4.4.b) (Ko and Jung, 2015). Because of low grain counts, ODF-J values may be artificially high for hornblende (Table 4.2).

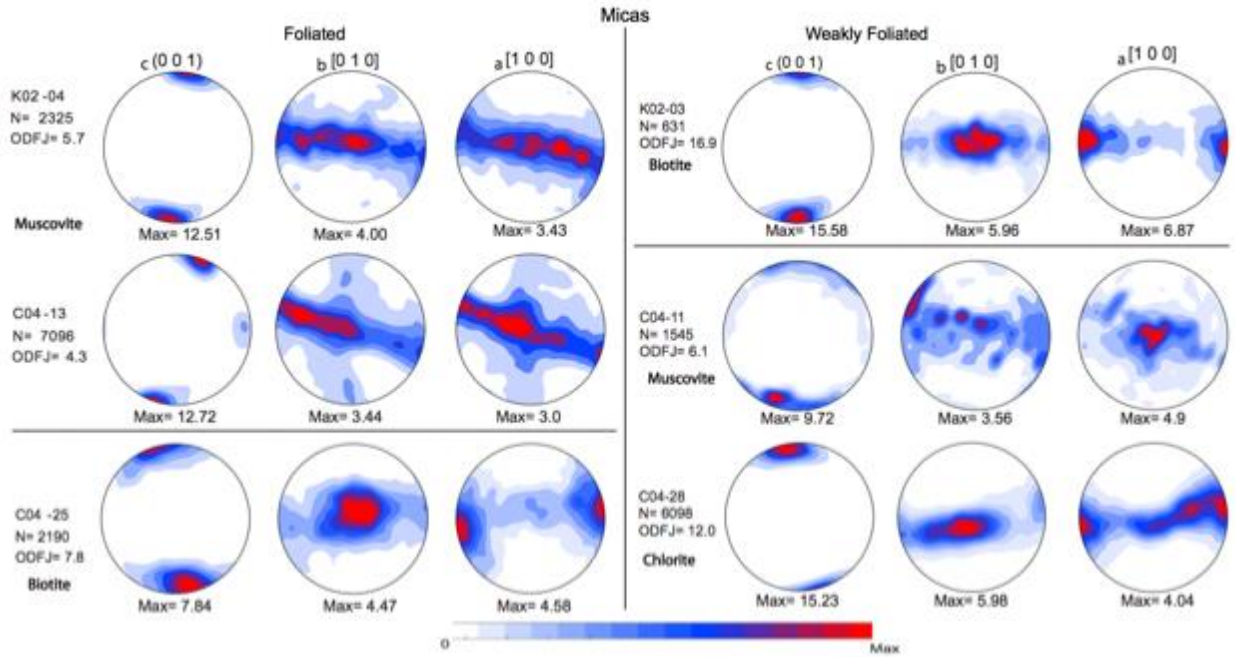

Figure 4.3. Pole figures of micas. Left, foliated group. Right, weakly foliated group.

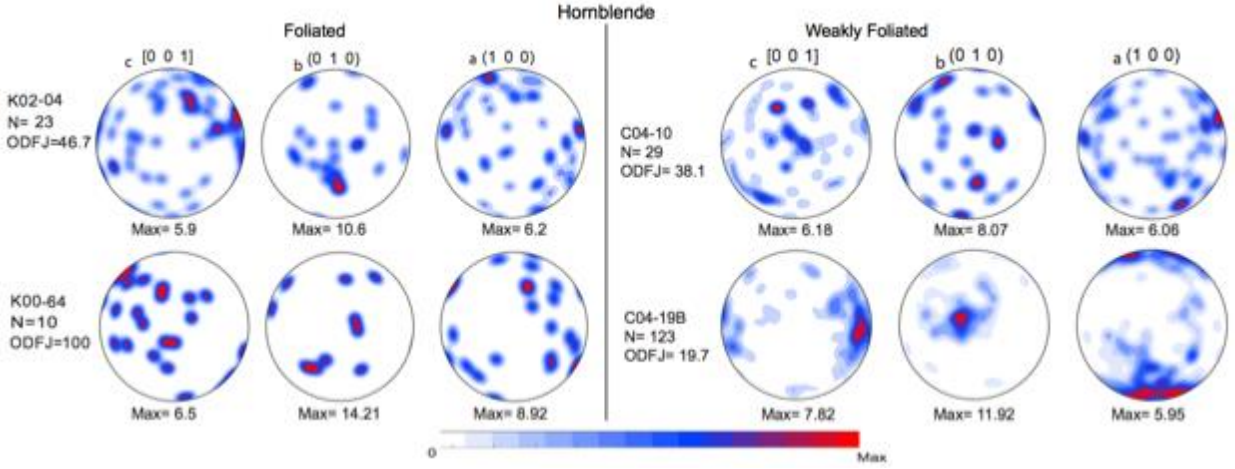

Figure 4.4 Pole figures of hornblende. Left, foliated group. Right, weakly foliated group.

4.2.6 Epidote

In the two samples that contain significant epidote, the epidote has relative strong CPOs with ODF-J values of 3.7 ± 2.5 (Table 4.2). Both samples are from the weakly foliated group, and have consistent CPOs with broad maxima of (001) poles perpendicular to the foliation, and a girdle distribution of [010] parallel to the lineation (Figure 4.5). The deformation mechanisms of epidote are not well studied, with only a few studies reporting epidote CPOs (Fujimoto et al., 2010).

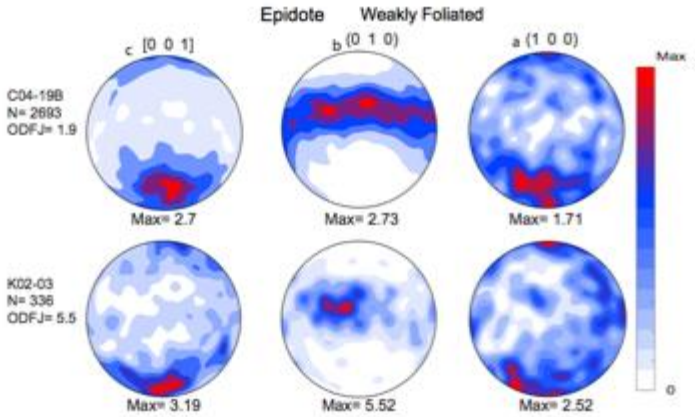

Figure 4.5 Pole figures of epidote for the weakly foliated group.

4.3 SEISMIC PROPERTIES

4.3.1 Isotropic Properties

On average the isotropic seismic properties are very similar for the foliated and weakly foliated samples, with the weakly foliated samples having slightly higher Vp and Vs wavespeeds (Table 4.3). Isotropic Vp ranges from 5.8 to 6.2 km/s over all samples, with the foliated samples averaging 6.0 ± 0.1 km/s, and the weakly foliated samples averaging 6.0 ± 0.1 km/s. The isotropic Vs ranges from 3.4 to 4.0 km/s, with the foliated samples averaging 3.5 ± 0.1 km/s, and

the weakly foliated samples averaging 3.8 ± 0.1 km/s. Vp/Vs ratios range from 1.5 to 1.7, with the foliated samples averaging 1.7 ± 0.0 and the weakly foliated sample averaging 1.6 ± 0.1.

Table 4.3. Isotropic and anisotropic seismic properties for the foliated and weakly foliated samples derived from the calculated elastic tensors. Uncertainties are bounds from Voigt and Reuss average tensors. Errors on averages are ± 1 standard deviation.

Sample#	VpIso (km/s)	VsIso (km/s)	VpVsIso	max(Vp) (km/s)	min(Vp) (km/s)	Avp (%)	MaxVs1 (%)	AvsMax (%)
foliated								
K02-04	$6.1_{-0.5}^{0.4}$	$3.7_{-0.3}^{0.3}$	$1.64_{-0.0}^{0.0}$	$6.58_{-0.5}^{0.4}$	$5.65_{-0.40}^{0.37}$	$15.08_{-0.1}^{0.2}$	$4.00_{-0.3}^{0.3}$	$15.53_{-1.1}^{1.8}$
C04-26	$6.1_{-0.6}^{0.6}$	$3.5_{-0.5}^{0.4}$	$1.72_{-0.0}^{0.1}$	$6.91_{-0.6}^{0.6}$	$5.31_{-0.46}^{0.42}$	$26.17_{-0.0}^{0.0}$	$3.98_{-0.5}^{0.4}$	$21.13_{-1.8}^{3.5}$
C04-25	$5.8_{-0.5}^{0.5}$	$3.4_{-0.5}^{0.4}$	$1.72_{-0.1}^{0.1}$	$6.21_{-0.5}^{-0.5}$	$5.41_{-0.45}^{0.41}$	$13.67_{-0.3}^{0.3}$	$3.64_{-0.4}^{0.4}$	$13.51_{-2.1}^{5.0}$
K00-64	$5.9_{-0.6}^{0.5}$	$3.4_{-0.5}^{0.4}$	$1.72_{-0.1}^{0.1}$	$6.36_{-0.6}^{0.5}$	$5.37_{-0.44}^{0.40}$	$16.80_{-0.5}^{0.6}$	$3.80_{-0.4}^{0.4}$	$19.60_{-3.3}^{5.6}$
C04-13	$5.9_{-0.5}^{0.5}$	$3.5_{-0.4}^{0.4}$	$1.67_{-0.0}^{0.1}$	$6.53_{-0.5}^{0.5}$	$5.50_{-0.47}^{0.43}$	$17.13_{-0.4}^{0.7}$	$3.92_{-0.4}^{0.4}$	$18.79_{-3.1}^{5.0}$
avg	5.9	3.5	1.7	6.5	5.5	17.8	3.9	17.7
s.d.	±0.1	±0.1	±0.1	±0.3	±0.1	±4.9	±0.2	±3.1
weakly-foliated								
K02-03	$6.0_{-0.3}^{0.3}$	$3.6_{-0.3}^{0.3}$	$1.63_{-0.0}^{0.0}$	$6.2_{-0.3}^{0.3}$	$5.9_{-0.3}^{0.3}$	$5.5_{-0.4}^{0.5}$	$3.9_{-0.3}^{0.2}$	$8.8_{-1.8}^{2.5}$
C04-19A	$5.8_{-0.5}^{0.5}$	$3.7_{-0.6}^{0.4}$	$1.59_{-0.0}^{0.1}$	$6.2_{-0.4}^{0.4}$	$5.5_{-0.5}^{0.4}$	$12.1_{-0.5}^{1.2}$	$4.1_{-0.4}^{0.4}$	$16.8_{-3.2}^{6.6}$
C04-19B	$6.2_{-0.3}^{0.3}$	$4.1_{-0.2}^{0.2}$	$1.53_{0.0}^{0.0}$	$6.4_{-0.3}^{0.3}$	$6.1_{-0.3}^{0.3}$	$3.8_{-0.1}^{0.4}$	$4.2_{-0.2}^{0.2}$	$5.6_{-0.3}^{0.4}$
C04-28	$6.1_{-0.3}^{0.3}$	$3.6_{-0.3}^{0.2}$	$1.70_{-0.2}^{0.0}$	$6.3_{-0.3}^{0.3}$	$6.0_{-0.3}^{0.3}$	$5.5_{-0.1}^{0.2}$	$3.8_{-0.2}^{0.2}$	$8.3_{-1.3}^{1.8}$
C04-9A	$6.0_{-0.3}^{0.3}$	$3.8_{-0.2}^{0.2}$	$1.59_{-0.0}^{0.0}$	$6.1_{-0.3}^{0.3}$	$5.9_{-0.3}^{0.3}$	$3.2_{-0.2}^{0.2}$	$3.9_{-0.2}^{0.2}$	$4.8_{-0.1}^{0.1}$
C04-10	$6.0_{-0.3}^{0.3}$	$3.8_{-0.3}^{0.3}$	$1.58_{-0.0}^{0.0}$	$6.1_{-0.3}^{0.3}$	$5.9_{-0.3}^{0.3}$	$4.4_{-0.2}^{0.5}$	$3.9_{-0.3}^{0.3}$	$7.0_{-1.1}^{1.7}$
C04-11	$6.1_{-0.4}^{0.4}$	$3.7_{-0.3}^{0.3}$	$1.64_{-0.0}^{0.0}$	$6.5_{-0.4}^{0.4}$	$5.7_{-0.3}^{0.3}$	$13.3_{-0.4}^{0.3}$	$4.0_{-0.3}^{0.3}$	$11.8_{-1.0}^{1.0}$
C04-15	$6.0_{-0.3}^{0.3}$	$3.8_{-0.2}^{0.2}$	$1.59_{-0.0}^{0.0}$	$6.1_{-0.3}^{0.3}$	$5.9_{-0.3}^{0.3}$	$2.7_{-0.0}^{0.0}$	$3.9_{-0.2}^{0.2}$	$4.1_{-0.0}^{0.3}$
C04-17	$5.9_{-0.4}^{0.4}$	$3.7_{-0.4}^{0.3}$	$1.59_{-0.0}^{0.1}$	$6.3_{-0.4}^{0.4}$	$5.6_{-0.4}^{0.4}$	$10.9_{-0.5}^{0.9}$	$4.0_{-0.3}^{0.3}$	$12.7_{-3.3}^{5.1}$
avg	6.0	3.8	1.6	6.2	5.8	6.8	4.0	8.9
s.d.	±0.1	±0.1	±0.1	±0.1	±0.2	±4.1	±0.1	±4.2

4.3.2 Magnitude of Seismic Anisotropy

The magnitude of seismic anisotropy in the foliated group ranges 15.1%-26.2% in AVp, and 15.5%-21.1% in AVs (Figure 4.6.a, Table 4.3). The maximum Vp in crenulated samples is roughly parallel to the crenulation lineation, or hinge line of the crenulations, and the minimum Vp is perpendicular to the foliation. The maximum AVs is found in a rough plane parallel to the overall foliation. The high AVs plane is slightly canted in most samples, and is narrower ~parallel to the crenulation lineation. The lowest AVs is found for waves propagating perpendicular to the foliation. The Vp/Vs1 ratio is also highest for propagation ~parallel to the crenulation lineation. On average, all of these samples have higher anisotropy than the weakly foliated group, probably due to their higher mica content.

The weakly foliated group has lower anisotropy, with AVp ranging 2.7%-13.3%, and AVs ranging 4.8%-16.8% (Figure 4.6.b, Table 4.3). The Vp maxima are generally parallel to the lineation, but the patterns of Vp with propagation direction are less consistent in this group than in the foliated group. The pattern in AVs is complex in many of the samples, with inconsistent relationship to Vp, however, in samples with higher anisotropy, the highest AVs is found in the same propagation directions as the highest Vp.

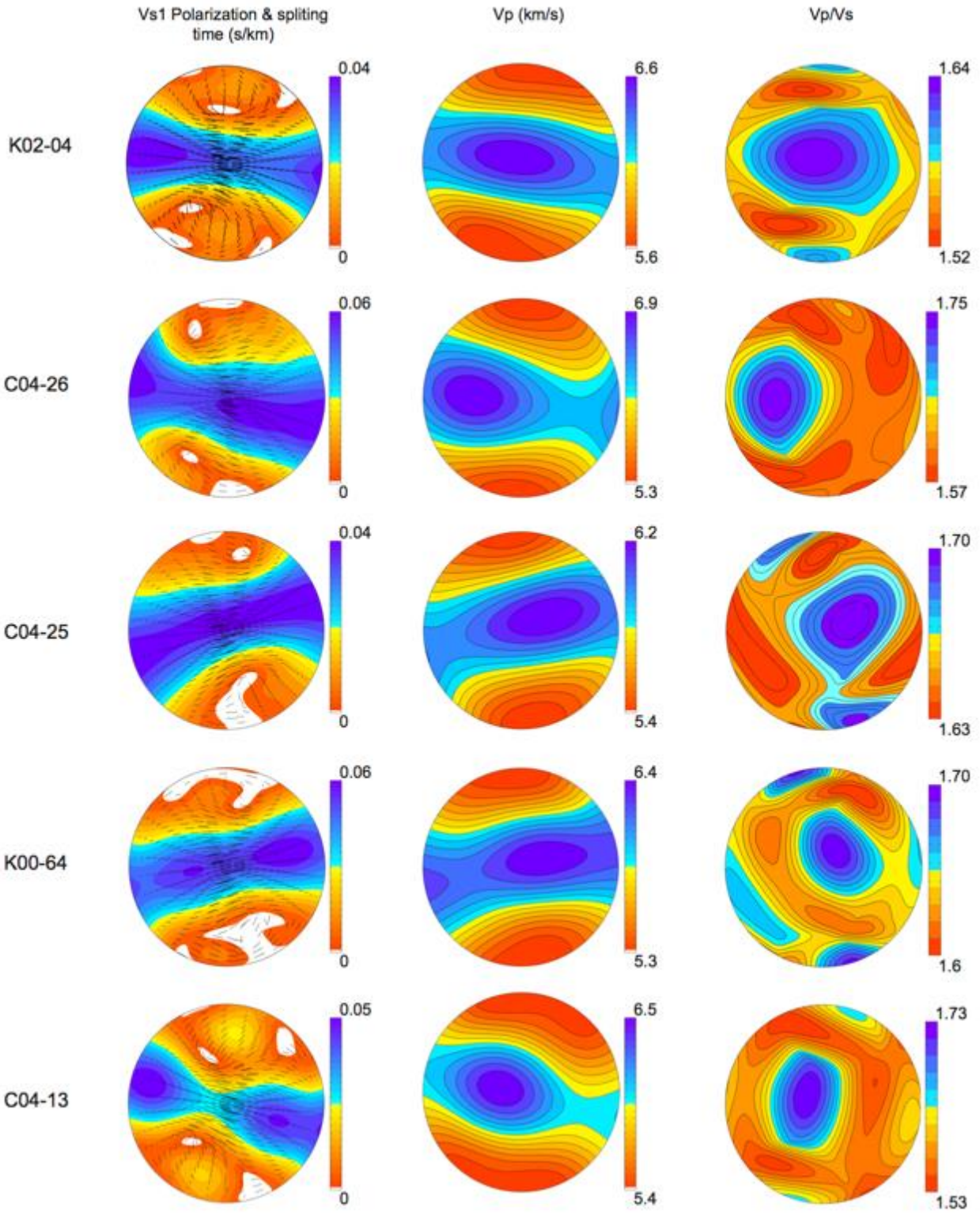

Figure 4.6.a. Velocity stereonets for the foliated samples. From left to right, polarization planes of the fast S-wave (Vs1), P-wave velocity, and Vp/Vs.

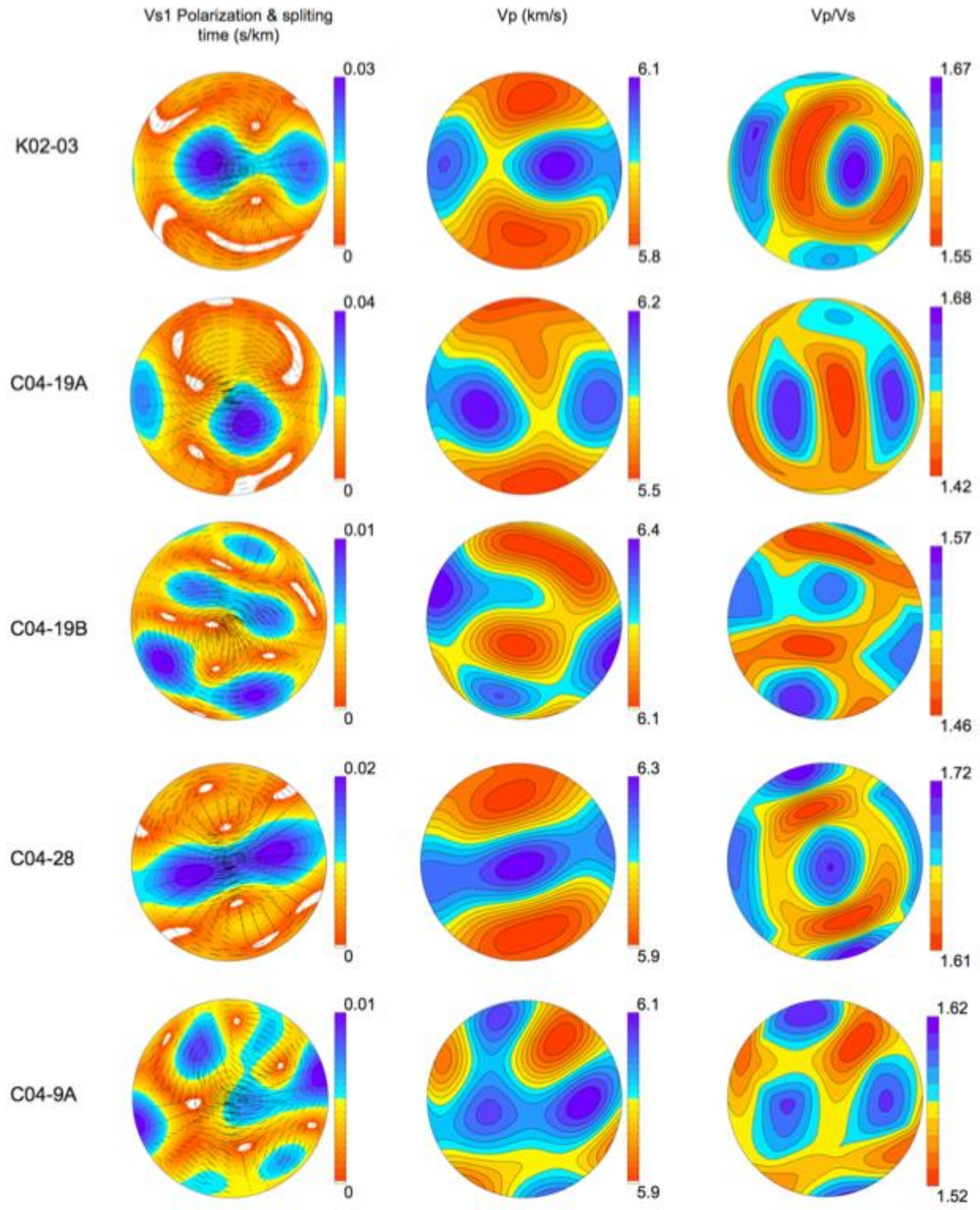

Figure 4.6.b. Velocity stereonets for the weakly foliated samples. From left to right, polarization planes of the fast S-wave (Vs1), P-wave velocity, and Vp/Vs.

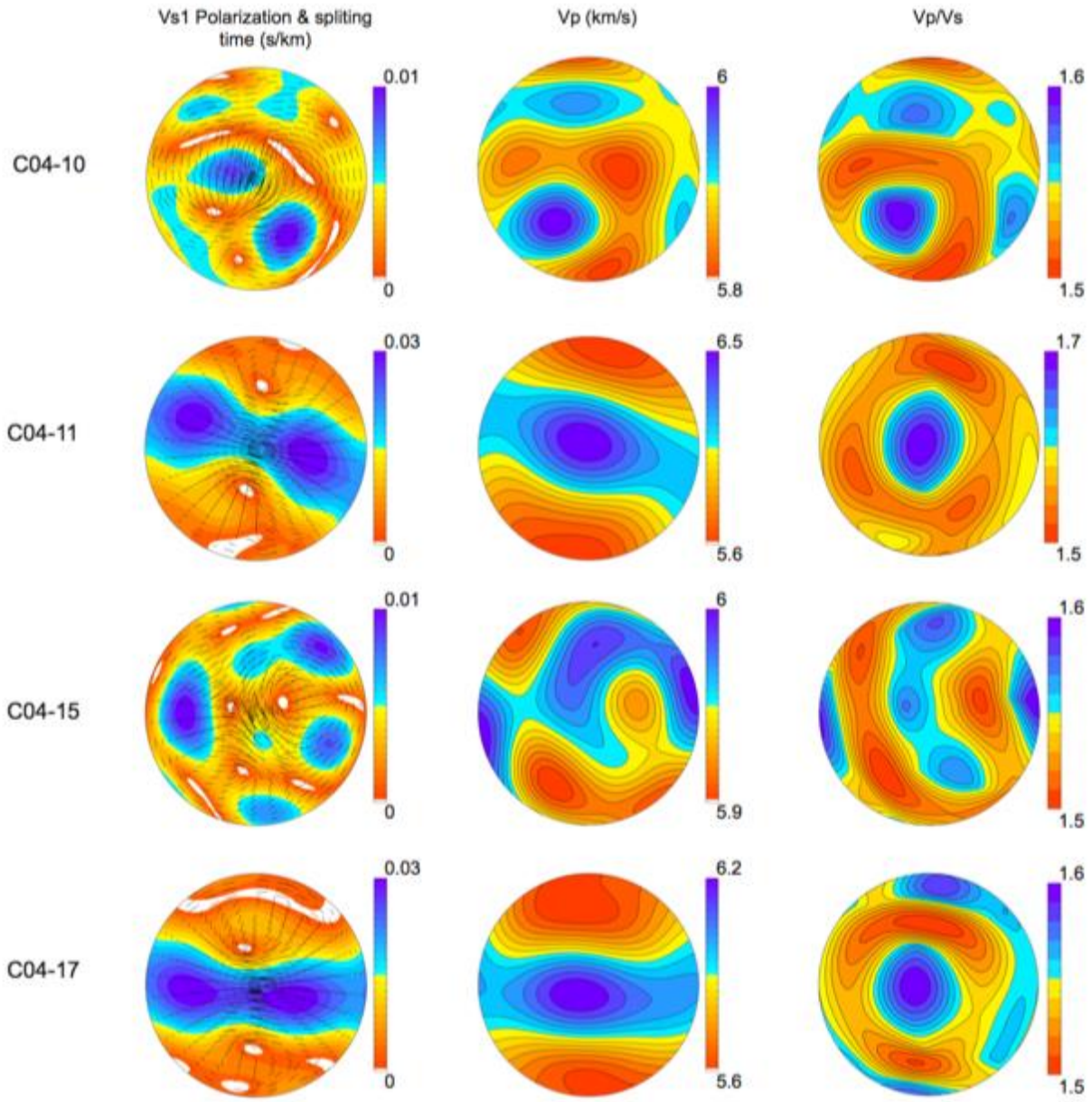

Figure 4.6.b. continued. Velocity stereonets for the weakly foliated samples. From left to right, polarization planes of the fast S-wave (Vs1), P-wave velocity, and Vp/Vs.

4.3.3 Elastic Tensor Symmetry

When decomposed into their symmetry components, all of the elastic tensors are dominated by an isotropic component. For the foliated group, the isotropic component ranges 80.7% - 88.8% (Table 4.4). The hexagonal component ranges 8.5% – 12.7% of the total tensor,

and orthorhombic symmetry accounts for 1% - 5%. The remaining symmetry components, tetragonal, monoclinic, and triclinic, account for 1%-2% of the total tensor.

In the weakly foliated group, the isotropic component of the tensor is higher, ranging from 89% – 96.7% (Table 4.4). In this group, the hexagonal symmetry component accounts for 3%-6% of the total tensor, and the orthorhombic component accounts for 0.5%-1.5%. The remaining three symmetry components account for 0.2%-1% of the total tensor. The symmetry components are not as consistent throughout this group as in the foliated group. In some samples, the anisotropy is dominated by hexagonal symmetry, and in others the anisotropy is dominated by a triclinic component. This group has more compositional variability than the foliated group, so this wider variation in symmetry is not surprising.

Table 4.4. Symmetry components of the calculated elastic tensors for each sample. Errors on averages are ± 1 standard deviation.

Sample	Isotropic	Hexagonal	Orthorhombic	Tetragonal	Monoclinic	Triclinic
foliated						
K02-04	87.1	9.7	1.6	0.0	0.7	0.9
C04-26	80.7	12.7	5.1	0.1	0.0	1.5
C04-25	88.8	8.5	1.7	0.0	0.0	1.0
K00-64	85.3	12.1	0.8	0.1	0.4	1.3
C04-13	85.8	8.4	3.8	0.4	0.7	0.9
average	85.6	10.3	2.6	0.1	0.4	1.1
± s.d.	3.1	2.0	1.8	0.2	0.3	0.3
weakly foliated						
K02-03	94.7	2.5	0.2	1.0	0.8	0.9
C04-19A	89.4	3.7	0.7	1.7	1.1	3.4
C04-19B	95.7	0.6	0.1	0.1	2.3	1.3
C04-28	94.5	3.6	0.1	0.2	0.6	1.0
C04-9A	96.4	0.4	0.9	0.2	0.1	2.0
C04-10	95.2	0.2	0.3	0.8	0.2	3.5
C04-11	89.8	6.4	2.0	0.4	0.1	1.4
C04-15	97.0	0.3	0.2	0.2	0.3	2.0
C04-17	90.1	6.7	1.2	0.1	0.3	1.6
average	93.6	2.7	0.6	0.5	0.6	1.9
± s.d.	3.0	2.6	0.6	0.6	0.7	0.9

CHAPTER 5:

DISCUSSION

5.1 HYPOTHESIS TESTING

The northern and the southern transects have a similar variety of rock types and deformational fabrics. We expect deformational fabric to control the strength of mineral CPOs, and thus the seismic anisotropy, in these samples, so we grouped the samples based on their fabric. We formulated 3 hypotheses that reflect this expectation: 1) the foliated group will have stronger mineral CPOs than the weakly foliated group, 2) the two transects will have similar average seismic properties, and 3) the foliated group will have higher seismic anisotropy than the weakly foliated group.

Hypothesis 1. *The foliated group will have stronger CPOs than the weakly foliated group.*

We used ODF-J values as a measure of CPO strength. ODF-J is the difference between the orientation distribution function calculated from our data that is limited to N grains, and a uniform orientation distribution function (Satsukawa et al., 2013). The actual ODF-J value has some dependence on mineral grain count, especially when less than about 200 grains are used. Therefore, to objectively compare ODF-J values from foliated and weakly foliated samples, the samples must have similar grain counts. Only two of the minerals analyzed, quartz and feldspar, have high enough grain counts in all of the samples to allow comparison between foliated and weakly foliated groups. Both quartz and feldspar have slightly higher ODF-J values for the foliated samples (quartz 2.4 ± 0.4, feldspar 3.3 ± 1.7) than the weakly foliated samples (quartz 2.3 ± 0.6, feldspar 3.2 ± 1.6) (Table 4.2). For hornblende, epidote, and pyrope we do not have enough grains to make objective comparisons between the two groups. The micas (biotite, muscovite, and chlorite) have grain counts over 100 in 6 out of 10 samples for biotite, 8 out 11

for muscovite, and 2 out of 4 for chlorite. For samples with grain counts above 100, the highest ODF-J is 10.41 for the foliated group (sample K00-64, biotite N= 876), which is lower than the highest mica ODF-J for the weakly foliated group at 16.86 (sample K02-03, biotite N=631). The average biotite ODF-J is slightly higher for the weakly foliated group than for the foliated group, but once again, we do not have high enough, or similar enough grain counts between the two groups to allow for a truly objective comparison of their ODF-J values.

The quartz and feldspar data support our hypothesis that samples with stronger deformational fabric will have stronger mineral CPOs. But without more data from the micas, which typically define the deformational fabric, we cannot support that conclusion with confidence. Therefore, our dataset does not support this hypothesis. More data, from mica and hornblende in particular, will likely provide a more robust conclusion. We think data collection methods could also be refined for the sparser minerals in these samples in order to collect more reliable data. In particular, we suggest collecting diffraction patterns on a grain-by-grain basis for these minerals, rather than using an automated mapping approach. This will improve that data first by ensuring that enough grains of these minerals are measured, and second, by selecting locations by hand, we can make sure diffraction patterns for these minerals are not collected from near grain boundaries.

Hypothesis 2. *The northern and southern transects will have similar seismic properties*

To approximate a bulk elastic tensor more consistent with seismic length-scales, we averaged the elastic tensors for each group for the northern and southern transects, and then we averaged those averages together. We expect these to show very little variation between the northern and southern transects (Table 5.1, Figure 5.1). The seismic anisotropy for the foliated averages in the northern and southern transects are very similar, 16.2% and 17% in AVp and

16.5% and 15% in AVs. For the weakly foliated averages, the variation is a little bit larger, but still not surprising, 5.1% and 4.6% in AVp and 5.6 – 6.3% in AVs. Overall the seismic properties for both transect do not present any significant variation. This observation suggests that the differences arise from compositional variation rather than sample location.

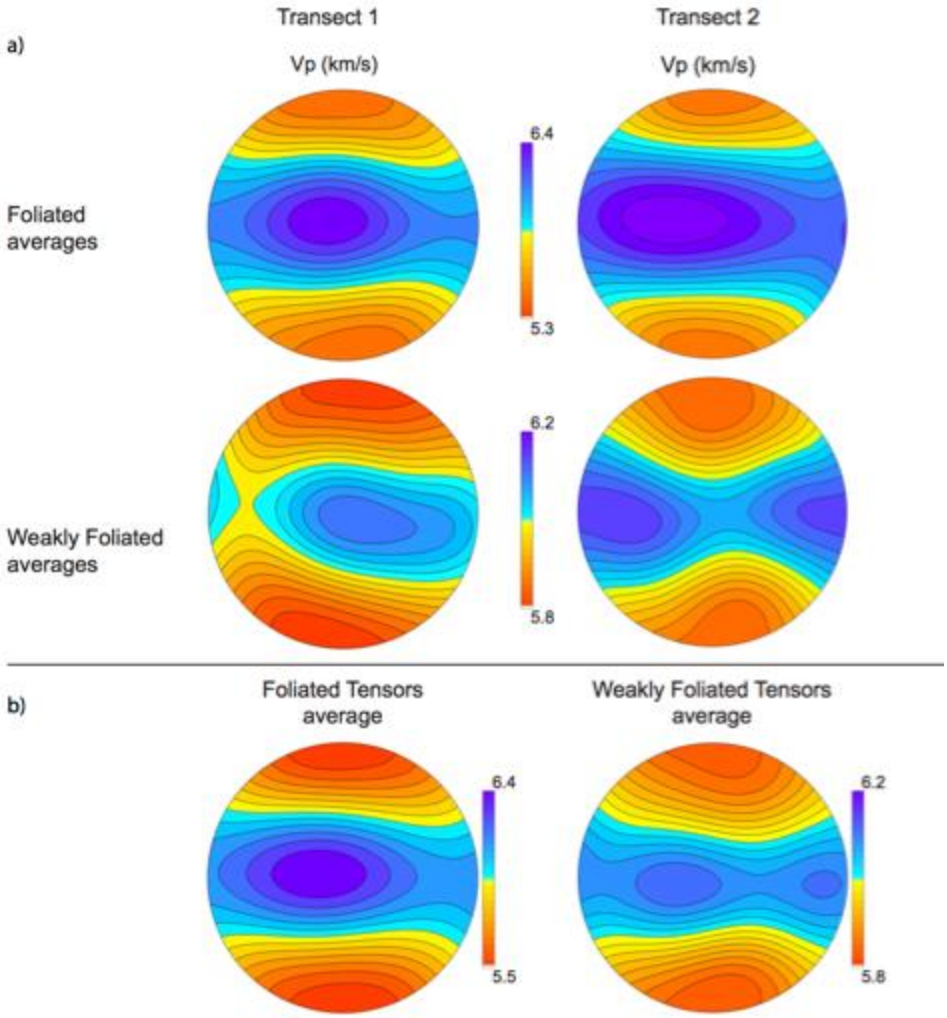

Figure 5.1. a) Northern (T1) and southern (T2) Vp averages for foliated and weakly foliated samples. b) Foliated and weakly foliated Vp averages.

Table 5.1. Isotropic and anisotropic seismic properties for the northern and southern transect with their foliated and weakly foliated tensors averages.

averages	VpIso	VsIso	VpVsIso	VpMax	VpMin	Avp	Vs1Max	AVsMax
T1foli	5.9	3.5	1.7	6.4	5.4	16.2	3.8	16.5
T2foli	6.0	3.5	1.7	6.5	5.5	17.0	3.9	15.0
T1wf	6.0	3.8	1.6	6.2	5.8	5.1	3.9	5.6
T2wf	6.0	3.7	1.6	6.2	5.9	4.6	3.9	6.3
T1T2foli	5.9	3.5	1.7	6.4	5.5	16.5	3.8	15.4
T1T2wf	6.0	3.7	1.6	6.1	5.9	4.4	3.9	5.6

Hypothesis 3. *The foliated group will have higher seismic anisotropy than the weakly foliated group.*

We hypothesized that the foliated samples would have higher seismic anisotropy than the weakly foliated samples because the schist fabric has well-developed foliation, which is defined by aligned micas. The foliated group must have significant amounts of mica, which has very high single crystal anisotropy, and the mica is also aligned to form the foliation fabric.

The foliated group does have higher average anisotropy (17.8 % ± 4.9) than the weakly foliated group (6.8 % ± 4.1). The foliated group also has higher mica content (48.4 % ± 21) than the weakly foliated group (13.3 % ± 15). The magnitude of seismic anisotropy in a sample is controlled by 3 factors: the crystallographic alignment of minerals (CPO), the single crystal anisotropy, and the modal proportion of minerals. Focusing on micas, the single crystal anisotropy for micas is very high and will not vary between the foliated and weakly foliated groups. The mica CPO strength was not measurably different between the two groups, and was strong (ODF-J > 6 for most samples) in both groups. The difference in anisotropy must therefore be related to the differences in mineral modal proportions between the two groups, for mica in particular.

Our dataset supports the hypothesis that foliated rocks will have higher anisotropy than weakly foliated rocks. Foliation, and schistocity in particular, is defined by the alignment of platy minerals, usually mica. Weakly foliated rocks still have aligned micas, but they don't have enough mica to develop a strong foliation fabric. The implication of this result combined with the fact that the mineral CPOs were similar between groups, is that visible deformation fabric may reflect mica content more than the actual finite strain accumulated in the sample.

5.2 ROLE OF MICA IN CRUSTAL DEFORMATION

The above discussion leads naturally to a discussion of the role of mica in crustal deformation. Micas are some of the weakest minerals found in the middle and lower crust (Shea and Kronenberg, 1992). Because of its low strength, the presence of mica has been suggested as a mechanism for strain localization in shear zones (Shea and Kronenberg, 1992). For example, if a rock's strength is a function of the strength of its constituent minerals, then rocks with a lot of mica will be weaker than those with less, and strain will be concentrated in the weaker materials. Mica also grows as a result of metamorphic reactions during deformation (Merriman et al., 1995), so deformation itself could act to increase mica content creating a sort of positive feedback.

It is clear from our results that mica content is controlling the magnitude of anisotropy in our sample set (Figure 5.2), but what is causing the variations in mica content? Is the mica in these samples growing as a result of metamorphism during deformation, or were there pre-existing variations in mineralogy? Is our foliated group simply the more deformed version of our weakly foliated group, or were there initial differences in composition that resulted in the foliated group being mechanically weaker? Within the context of the Appalachian Mountains, which are composed mostly of metamorphosed sedimentary sequences, both scenarios are

equally likely. But in some tectonic environments, variations in seismic anisotropy may be diagnostic of strain localization.

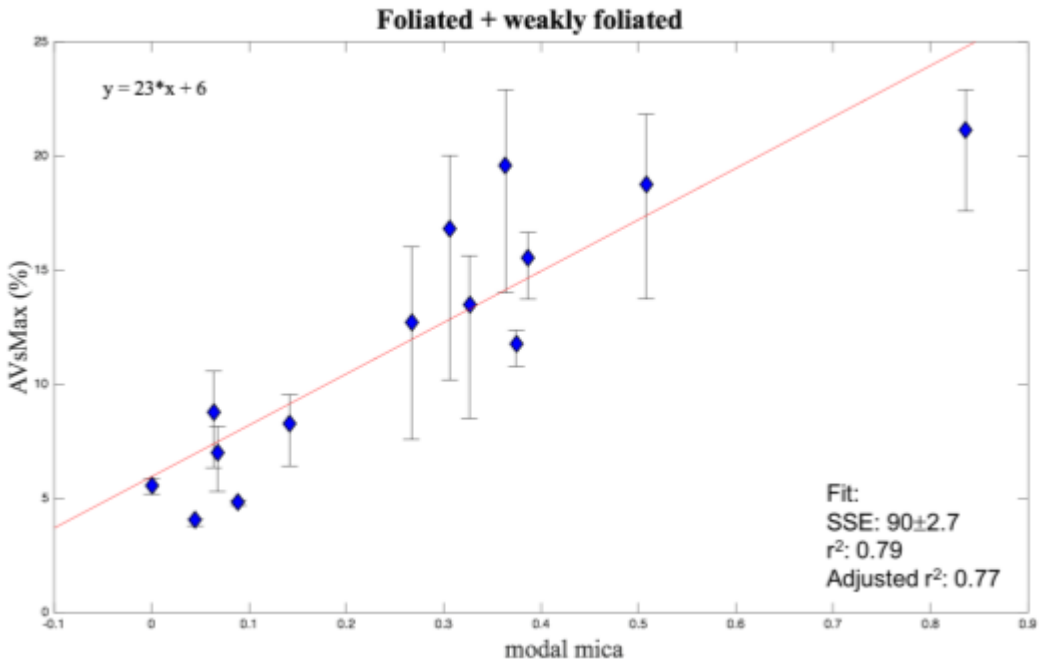

Figure 5.2. Anisotropy Vs. modal mica with positive linear correlation.

5.3 ROLE OF QUARTZ AND FELDSPAR IN SEISMIC ANISOTROPY

Quartz is one of the most abundant crustal minerals, with interpretations of its influence ranging from having no influence on bulk anisotropy, to having an important influence on seismic anisotropy (Ward, 2010). In contrast to mica, which serves to increase anisotropy, quartz and feldspar are both thought to dilute, or weaken anisotropy (Jones and Nur, 1982); (Weiss et al., 1999). Our dataset supports this idea (Figure 5.2, 5.3), previous studies suggest that samples with aligned quartz, the quartz decreases the overall anisotropy produced by aligned mica, and this relationship can be useful when interpreting crustal deformation (Ward et al., 2012).

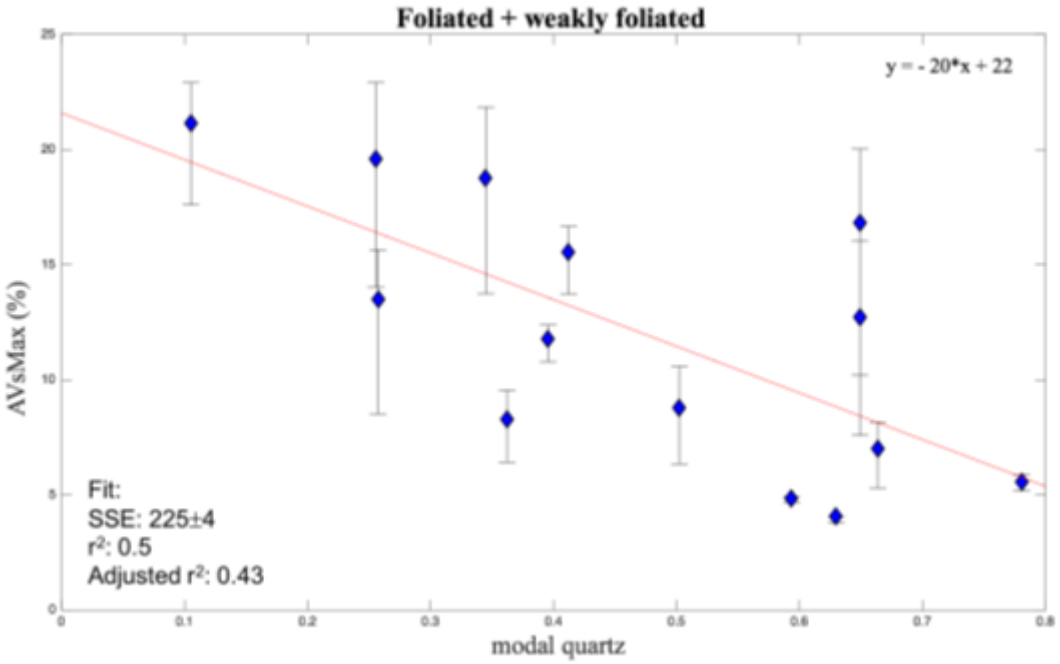

Figure 5.3. Anisotropy Vs. modal quartz with negative correlation.

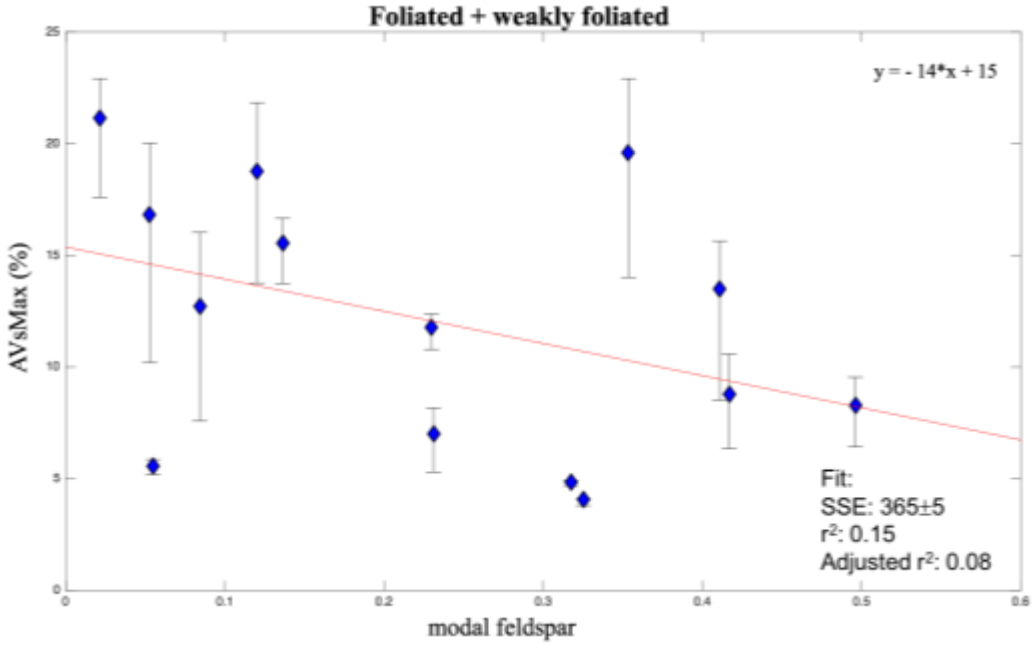

Figure 5.4. Anisotropy Vs. modal feldspar with negative correlation.

Rocks that have a high modal abundance of feldspar have deformation mechanisms that are not fully understood, CPOs found in these rocks are generally weak due to deformation

processes that do not produce strong crystallographic fabrics, therefore, these poor CPOs in general contribute little to bulk seismic anisotropy (Llana-Fúnez and Brown, 2012). The samples with more quartz and feldspar have lower seismic anisotropy than those with less. When compared with common CPOs for mica or hornblende, quartz and feldspar both have weak CPOs. This is true for our samples as well, where quartz and feldspar have much lower ODF-J values than mica. But there are examples of quartz-rich rocks that have high anisotropy, mainly quartzites (Ward et al., 2012).

5.4 CRUSTAL AVERAGE TENSORS

In order to approximate the bulk elastic tensor that seismic waves will be sensitive to, we calculated a couple of crustal average tensors. First, we computed an average for each group (Figure 5.1), then we computed a bulk average including all of the samples. The most accurate average for this region will have the two rock groups averaged according to their actual proportions in the area (40% foliated – 60% weakly foliated) (Figure 5.5).

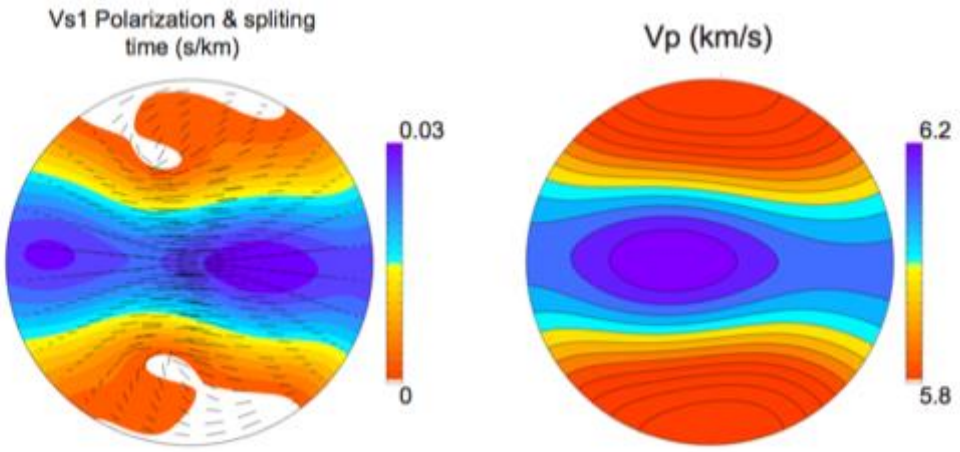

Figure 5.5. Regional average of the foliated and weakly foliated groups. Foliated rocks covers 40% of the map area and weakly foliated covering 60% of the map area.

Most of the studies of seismic anisotropy in the southern Appalachians have been done from observations of null and non-null SKS splitting using temporary seismic deployments

across the region. These observations of anisotropy can provide us with information about past and present mantle deformation, as well as the lithospheric deformation and asthenospheric flow contribution to regional anisotropy (Savage, 1999; Wagner et al., 2012). In this region the magnitude of the observed SKS splitting is about 1 second or more. Seismologist believe that the crustal contribution is only about a tenth of a second of shear-wave splitting out of that 1 second (Wagner et al., 2012). In contrast, our results suggest that if the average crust is 40% foliated rocks and 60% weakly foliated rocks (Figure 5.5), with 10-15 km of vertical or steeply dipping foliation, the crust would contribute at least 0.3 s to the overall splitting. If the average crust contains slightly more foliated rocks than weakly foliated, as in figure 5.6, then 10 km of steeply dipping foliation would contribute almost half a second (0.4 s) of the observed 1 s SKS splitting time, or 40% of the signal would be from the crust. This is very significant for studies using SKS splitting observations to interpret mantle flow patterns. Therefore, it is important to consider, and account for the potential anisotropic signal of the crust in areas where there are highly foliated rocks, rich in mica, and steeply dipping foliations, such as would be expected in orogenic terranes..

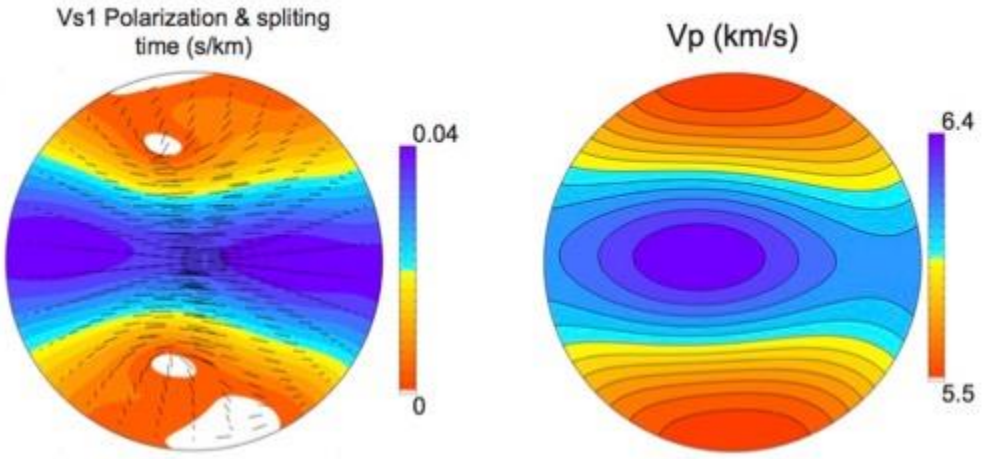

Figure 5.6. Regional average of the foliated group with a shear wave splitting contribution of 0.4s.

5.5 SYMMETRY OF ELASTIC TENSORS

Many seismic methods for measuring seismic anisotropy use an assumption of simplified elastic symmetry. The symmetry is assumed to be hexagonal, or transversely isotropic, which is to say there is one unique direction about which all velocities are equal. For the crust, the assumption is that the unique axis is the slowest seismic velocity, and the maximum velocity is found within the plane perpendicular to the unique axis. The results from our dataset are pretty consistent with this assumption. All of the samples have a strong component of hexagonal symmetry, and they all have a slow unique axis of anisotropy. Even though the dataset is mostly consistent with commonly used symmetry assumptions, the assumption of hexagonal symmetry is clearly an oversimplification of the true symmetry of the rocks. There is another important distinction. Most seismic studies assume elliptical transverse isotropy, which is the case when all of the phase velocity cross-sections are purely elliptical. Our samples show a shear wave cross-over point, where there is a 90˚ rotation in the polarization direction of the fast shear wave at a propagation direction between 45-20˚ from the symmetry axis. This is indicative of non-elliptical hexagonal symmetry (Okaya and Christensen, 2002). The effects of assuming elliptical symmetry rather than the more realistic, but still over-simplified, non-elliptical transverse isotropy, have not been fully determined, but we expect this assumption to result in inaccurate determinations of magnitude of anisotropy.

CHAPTER 6:

CONCLUSIONS

We investigated the crystallographic preferred orientation and the seismic properties of lower-crustal rocks by combining two different methods: 1) crystal orientations measurements, and 2) elastic tensor calculations based on modal proportions, CPOs of major minerals, single crystal elastic tensors, and densities. We can conclude that:

1. ODF-J number mismatches of micas between the foliated and the weakly foliated groups represented a limitation in our study because we were not able to objectively compare the strength of CPOs between our two groups; however, with more data from the micas with high enough grain counts, we conclude that foliated rocks that contain high mica content would present stronger mineral CPO because micas present high single crystal anisotropy and overall strong crystallographic preferred orientation.

2. Seismic velocities calculated from mineral CPO and individual elastic constants are representative of true rock properties. EBSD measurements demonstrate that seismic anisotropy varies between our two groups because of changes in mineralogy. Schist samples show much higher Vp anisotropy (17.8 ± 4.9) than the other metamorphic rocks (6.8 ± 4.1) such as phyllites and slates in which the constituent minerals have geometrically complex seismic properties that produce low anisotropy and nearly isotropic properties.

3. The degree of anisotropy for the schist samples is a function of the mica content, CPO strength, and strain geometry. All of the schist samples show high Vp velocity within the foliation plane, indicating that their seismic properties are hexagonal rather than purely isotropic.

4. Equally important is the need to recognize that the crust can have as much influence on overall anisotropy as the mantle. For example, if the continental crust is dominated by the foliated rocks

in this study with a steeply dipping foliation and a thickness of ~10 km, then the crust would contribute about ~40% of the magnitude of the observed SKS splitting measurements in the southern Appalachians region.

Future work will focus on developing receiver function models using our observed polarization and splitting time to develop an integrated technique to provide accurate estimates of crustal anisotropy.

REFERENCES

Brocher, T. M., and Christensen, N. I., 1990, Seismic anisotropy due to preferred mineral orientation observed in shallow crustal rocks in southern Alaska: Geology, v. 18, no. 8, p. 737-740.

Browaeys, J. T., and Chevrot, S., 2004, Decomposition of the elastic tensor and geophysical applications: Geophysical Journal International, v. 159, no. 2, p. 667-678.

Brownlee, S. J., Hacker, B. R., Salisbury, M., Seward, G., Little, T. A., Baldwin, S. L., and Abers, G. A., 2011, Predicted velocity and density structure of the exhuming Papua New Guinea ultrahigh-pressure terrane: Journal of Geophysical Research: Solid Earth, v. 116, no. B8.

Carpenter, R. H., 1970, Metamorphic history of the Blue Ridge province of Tennessee and North Carolina: Geological Society of America Bulletin, v. 81, no. 3, p. 749-762.

Christensen, N. I., 1966, Shear wave velocities in metamorphic rocks at pressures to 10 kilobars: Journal of Geophysical Research, v. 71, no. 14, p. 3549-3556.

-, 1982, Seismic velocities: Handbook of physical properties of rocks, v. 2, p. 1-228.

Erdman, M. E., Hacker, B. R., Zandt, G., and Seward, G., 2013, Seismic anisotropy of the crust: electron-backscatter diffraction measurements from the Basin and Range: Geophysical Journal International, v. 195, no. 2, p. 1211-1229.

Fujimoto, Y., Kono, Y., Hirajima, T., Kanagawa, K., Ishikawa, M., and Arima, M., 2010, P-wave velocity and anisotropy of lawsonite and epidote blueschists: Constraints on water transportation along subducting oceanic crust: Physics of the Earth and Planetary Interiors, v. 183, no. 1, p. 219-228.

Godfrey, N. J., Christensen, N. I., and Okaya, D. A., 2000, Anisotropy of schists: Contribution of crustal anisotropy to active source seismic experiments and shear wave splitting observations: Journal of Geophysical Research: Solid Earth, v. 105, no. B12, p. 27991-28007.

Hatcher, R. J., 1972, Developmental model for the southern Appalachians: Geological Society of America Bulletin, v. 83, no. 9, p. 2735-2760.

-, 1988, Bedrock geology and regional geologic setting of Coweeta Hydrologic Laboratory in the eastern Blue Ridge, Forest hydrology and ecology at Coweeta, Springer, p. 81-92.

-, 2005, Southern and central Appalachians: Encyclopedia of geology, p. 72-81.

Ji, S., Shao, T., Michibayashi, K., Oya, S., Satsukawa, T., Wang, Q., Zhao, W., and Salisbury, M. H., 2015, Magnitude and symmetry of seismic anisotropy in mica-and amphibole-bearing metamorphic rocks and implications for tectonic interpretation of seismic data from the southeast Tibetan Plateau: Journal of Geophysical Research: Solid Earth, v. 120, no. 9, p. 6404-6430.

Jones, T., and Nur, A., 1982, Seismic velocity and anisotropy in mylonites and the reflectivity of deep crystal fault zones: Geology, v. 10, no. 5, p. 260-263.

Keller, R. R., and Geiss, R. H., 2012, Transmission EBSD from 10 nm domains in a scanning electron microscope: Journal of Microscopy, v. 245, no. 3, p. 245-251.

Ko, B., and Jung, H., 2015, Crystal preferred orientation of an amphibole experimentally deformed by simple shear: Nature communications, v. 6.

Lesure, F. G., 1968, Mica deposits of the Blue Ridge in North Carolina: US Government Printing Office, 2330-7102.

Llana-Fúnez, S., and Brown, D., 2012, Contribution of crystallographic preferred orientation to seismic anisotropy across a surface analog of the continental Moho at Cabo Ortegal, Spain: Geological Society of America Bulletin, v. 124, no. 9-10, p. 1495-1513.

Long, M. D., and Becker, T. W., 2010, Mantle dynamics and seismic anisotropy: Earth and Planetary Science Letters, v. 297, no. 3, p. 341-354.

Mainprice, D., 1990, A FORTRAN program to calculate seismic anisotropy from the lattice preferred orientation of minerals: Computers & Geosciences, v. 16, no. 3, p. 385-393.

Mainprice, D., Bachmann, F., Hielscher, R., and Schaeben, H., 2015, Descriptive tools for the analysis of texture projects with large datasets using MTEX: strength, symmetry and components: Geological Society, London, Special Publications, v. 409, no. 1, p. 251-271.

Mainprice, D., and Humbert, M., 1994, Methods of calculating petrophysical properties from lattice preferred orientation data: Surveys in Geophysics, v. 15, no. 5, p. 575-592.

Merriman, R., Roberts, B., Peacor, D., and Hirons, S., 1995, Strain-related differences in the crystal growth of white mica and chlorite: a TEM and XRD study of the development of metapelitic microfabrics in the Southern Uplands thrust terrane, Scotland: Journal of Metamorphic Geology, v. 13, no. 5, p. 559-576.

Naus-Thijssen, F. M. J., 2011, Crenulation cleavage development and the influence of rock microstructure on crustal seismic anisotropy.

Okaya, D. A., and Christensen, N. I., 2002, Anisotropic effects of non-axial seismic wave propagation in foliated crustal rocks: Geophysical Research Letters, v. 29, no. 11.

Prior, D. J., and Wheeler, J., 1999, Feldspar fabrics in a greenschist facies albite-rich mylonite from electron backscatter diffraction: Tectonophysics, v. 303, no. 1, p. 29-49.

Satsukawa, T., Ildefonse, B., Mainprice, D., Morales, L., Michibayashi, K., and Barou, F., 2013, A database of plagioclase crystal preferred orientations (CPO) and microstructures-implications for CPO origin, strength, symmetry and seismic anisotropy in gabbroic rocks: Solid Earth, v. 4, no. 2, p. 511.

Savage, M., 1999, Seismic anisotropy and mantle deformation: what have we learned from shear wave splitting?: Reviews of Geophysics, v. 37, no. 1, p. 65-106.

Shea, W. T., and Kronenberg, A. K., 1992, Rheology and deformation mechanisms of an isotropic mica schist: Journal of Geophysical Research: Solid Earth, v. 97, no. B11, p. 15201-15237.

Valcke, S., Casey, M., Lloyd, G., Kendall, J.-M., and Fisher, Q., 2006, Lattice preferred orientation and seismic anisotropy in sedimentary rocks: Geophysical Journal International, v. 166, no. 2, p. 652-666.

Wagner, L. S., Long, M. D., Johnston, M. D., and Benoit, M. H., 2012, Lithospheric and asthenospheric contributions to shear-wave splitting observations in the southeastern United States: Earth and Planetary Science Letters, v. 341, p. 128-138.

Ward, D., Mahan, K., and Schulte-Pelkum, V., 2012, Roles of quartz and mica in seismic anisotropy of mylonites: Geophysical Journal International, v. 190, no. 2, p. 1123-1134.

Ward, D. E., 2010, The relative influence of quartz and mica on crustal seismic anisotropy.

Weiss, T., Siegesmund, S., Rabbel, W., Bohlen, T., and Pohl, M., 1999, Seismic velocities and anisotropy of the lower continental crust: a review: Seismic Exploration of the Deep Continental Crust, p. 97-122.

ABSTRACT

CHARACTERIZING MINERAL CRYSTALLOGRAPHIC PREFERRED ORIENTATIONS (CPOS) ALONG THE EASTERN NORTH AMERICAN MARGIN IN THE SOUTHERN APPALACHIANS: IMPLICATIONS FOR MIDDLE AND LOWER CRUSTAL SEISMIC ANISOTROPY

By

LAURA ROBLES

May, 2017

Advisor: Dr. Sarah Brownlee

Major: Geology

Degree: Master of Science

The Southern Appalachians Mountains have a complex and distinctive tectonic history, characterized by structural deformation extending from late Precambrian throughout the Paleozoic. The Southern Appalachians, known as the Blue Ridge of western North Carolina and eastern Tennessee, is mainly composed of schists and gneisses, granitic and ultramafic intrusives, as well as a sedimentary portion. The main tool for understanding the composition and structure of the deeper parts of the crust that cannot be directly sampled by seismology. Seismic anisotropy is the directional dependence of seismic velocity, and it is an invaluable tool for interpreting the development of sub-surficial dynamics. Seismic anisotropy can have a number of controlling parameters including shear strain, mineral grain aspect ratios, and aligned cracks, and crystallographic preferred orientations. If these parameters are known, we can use anisotropy to constrain lower and middle crustal composition. In an effort to characterize the southern Appalachian region's compositional and structural variability, we will present results from calculations of elastic tensors derived from electron backscatter diffraction (EBSD) data from a variety of metamorphic rocks with different mineral compositions. Here we will report

analyses from 14 samples that are distributed into two transects across the Blue Ridge. Our goal is to address how deformational fabric controls the strength of mineral CPOs and thus seismic anisotropy.

AUTOBIOGRAPHICAL STATEMENT

Laura Robles attended Oriente University in Venezuela and received her bachelor's degree in Geological Engineering in 2011. In 2013 she moved to the US to pursue a Master's of Science degree in Geology at Wayne State University.